JOURNAL OF GEOPHYSICAL RESEARCH, VOL. 92, PAGES 2385-2407, MARCH 1, 1987

Plasma Observations at the Earth's Magnetic Equator

R. C. OLSEN, S. D. SHAWHAN, D. L. GALLAGHER, J. L. GREEN,
C. R. CHAPPELL, AND R. R. ANDERSON

The magnetic equator provides a unique location for thermal plasma and plasma wave measurements. Plasma populations are found to be confined within a few degrees latitude of the equator, particularly the ions. The equatorially trapped ion population is found to be primarily hydrogen and we find little evidence for preferential heating of heavier ions. Helium is occasionally found to be heated along with the protons, and forms about 10% of the equatorially trapped populations at such times, similar to the percentage of He+ in the cold, core plasma of the plasmasphere. One case of a heated O^+ component was found; at the 0.1% level it generally comprises in the outer plasmasphere core plasma. The heated H^+ ions can be characterized by a bi-Maxwellian with $kT_{\|}$ = 0.5–1.0 eV and $kT_{\perp}$ = 5–50 eV, with a density of 10–100 cm^{-3}. The total plasma density, as inferred from the plasma wave instrument measurements of the upper hybrid resonance (UHR) is relatively constant with latitude, occasionally showing a local minimum at the magnetic equator, even though the ion flux has increased substantially. The first measurements of the equatorially trapped plasma and coincident UHR measurements show that the trapped plasma is a feature of the plasmapause region, found at total plasma densities of 20–200 cm^{-3}. The warm, trapped plasma is found in conjunction with equatorial noise, a plasma wave feature found at frequencies near 100 Hz, with a broad spectrum generally found between the proton gyrofrequency at the low frequency edge and the geometric mean gyrofrequency at the high frequency edge. This latter frequency is generally the lower hybrid resonance (LHR) for a proton-electron plasma. Sharp spatial boundaries are occasionally found with latitude, delimiting the equatorially trapped plasma. In such cases, the equator is a region with a relative minimum in density, and it appears that field-aligned ions found at higher latitudes are "bounced" from these boundaries, indicating a positive plasma potential of a volt or two in the equatorial region.

INTRODUCTION

Plasma and wave characteristics at the magnetic equator are important to our understanding of the magnetosphere. A number of wave-particle interactions seem to be localized at or near the equator. GEOS 1 and 2 observations published by *Young et al.* [*1981*] and *Roux et al.* [*1982*] showed evidence of ion cyclotron waves and heated plasma. with a strong dependence inferred from the mass composition of the cold ion population. In particular, they found that relatively high He^+/H^+ ratios (0.1 to 0.5) were required to obtain wave activity, that the observed wave frequencies were strongly ordered by the helium gyrofrequency, and that helium was the ion which was primarily heated. *Mauk* [*1982*] has studied these processes from the perspective provided by ATS 6 particle and magnetometer data. The complementary case of electron heating due to electron gyroharmonics has been shown using GEOS data by *Wrenn et al.* [*1979*] and *Gough et al.* [*19791.*

Olsen [*1981*] showed ion and wave data from the SCATHA satellite between 5.5 and 6.6 RE at the magnetic equator. and inferred that a cold isotropic background or a cold field-aligned population (E 5 eV) was being heated transverse to the magnetic field line up to energies of hundreds of electron volts, with the peak ion flux typically between 50 and 100 eV. Corresponding increases in the electric field amplitudes to between 0.1 and 1.0 mV/m in the 20- to 200-Hz frequency range were also found. Electron heating was also inferred at the equator. in agreement with the observations by *Wrenn et al.* [*1979*]. *Quinn and Johnson* [*1982*] used mass spectrometer data from SCATHA to show that the ion composition of the equatorially trapped plasma population was primarily hydrogen above 100 eV, and inferred from the distribution functions that the bulk of the ions below 100 eV were also hydrogen.

The 20- to 200-Hz wave population associated with the heated plasma was identified as "equatorial noise." first reported by *Russell et al.* [*1970*] using magnetometer measurements in the 1- to 1000-Hz frequency range. The spectrum of the equatorial noise as reported by Russell et al. generally appeared in the 5- to 200-Hz range. These OGO 3 magnetometer measurements and wideband wave data from the Hawkeye and IMP 6 satellites [*Gurnett. 1976*] show that the equatorial noise spectrum has a fine structure at or near harmonics of the proton gyrofrequency, with indications of additional fine structure. *Russell et al*. declined to interpret the data as evidence of ion gyroharmonics, however. They found the signals to be propagating nearly perpendicular to B. and concluded that they could be in bounce resonance with energetic electrons. *Gurnett* presented electric field data (and referred to magnetic loop data) taken from L = 2.5 to 3.5, at all local times. *Gurnett* argued against *Russell et al*.'s interpretation of the wave structure as interaction with electron bounce resonance, and noted that the fine structure could be explained as the helium and oxygen gyro-frequencies. *Gurnett* suggested that the structure, and fine structure, were the result of resonance with energetic ions (i.e., H^+, He^+, and perhaps O^+) which had gyroradii comparable to the perpendicular wavelength of the waves. *Perraut et al.* [*1982*] show GEOS observations of these waves, distinguishing carefully between ion cyclotron waves (ICW) which are found below the proton gyrofrequency and propagate parallel to B. and the magnetosonic waves (MSW) which are found above the proton gyrofrequency, and propagate perpendicular to B. The former are the waves extensively studied by *Young et al.* [*1981*] and *Roux et al.* [*1982*]. The latter are more apparent in the DE data. Perraut et al. argued that much of the harmonic structure seen in the MSW's is due to non-linear coupling. Combinations of fundamentals near the proton gyrofrequency produce an abundance of fine structure. They find MSW's at all local times, peaking shortly after local noon. and with a minimum at local dawn. (By comparison with the present study, this is at least partly a symptom of being well outside the plasmasphere at local dawn on a. geosynchronous satellite.) *Perraut et al.* link the MSW's to proton "ring" distributions. These are ring current distributions with local minima between 1 and 10 keV, due to magnetospheric convection, and local maxima at 20-40 keV

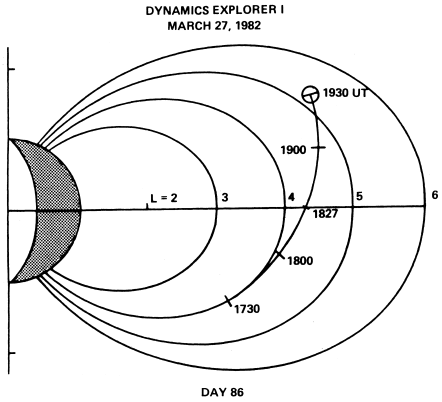

Fig. 1. Orbit plot for March 27, 1982 (day 86), in solar magnetic coordinates. The orbit has been rotated into a common plane at the local time of 2230.

It appears that the equatorial noise is a generalized ion Bernstein mode with the magnetic component of the wave parallel to the quasi-static magnetic field (i.e., compressional in B) and the electric component perpendicular to B [*Fredericks, 1968; Gurnett, 1976*]. *Rauch and Roux* [*1982*] have performed ray tracing calculations which show the MSW, or Bernstein mode, propagates radially outward, and is limited to within a few degrees of the magnetic equator by index of refraction effects (A. Roux, private communication, 1983).

The purpose of this paper is to show new observations of particle and wave data from the magnetic equator from the Dynamics Explorer I (DE l) spacecraft. The polar orbit of DE 1 provides a unique perspective on these equatorial phenomena. Orbital trajectories during the spring of 1982 were at nearly constant L values across the magnetic equator. These orbits result in clear latitudinal profiles of the plasma and wave characteristics, without the local time and radial variations of previous satellites. The new measurements demonstrate that the equatorial plasma population is predominantly hydrogen and that the enhanced ion fluxes observed at the equator occur without an increase in the total plasma density. Total plasma densities for these populations are given for the first time. In the first example, our "classical" case is shown, illustrating what we consider to be a typical case of trapped plasma and equatorial noise. The second case illustrates a time when the equatorially trapped plasma is bounded in latitude by regions of cold isotropic plasma. The third shows an example where only H^+ is heated. The fourth example further demonstrates the sharp spatial boundaries near the plasmapause. and the apparent reflection of field-aligned ions from the equator. The final case makes use of ISEE 1 radial density profiles to resolve some of the ambiguity between radial and latitudinal variations. These examples are followed by a statistical summary of the observations of equatorially trapped plasma.

INSTRUMENTATION

DE 1 was launched on August 3, 1981, into an elliptical polar orbit with apogee at 4.7 RE. It spins with a 6-s period, with its spin axis perpendicular to the orbit plane of the satellite. The orbital period is approximately 7.5 hours. Data for this study are taken from the retarding ion mass spectrometer (RIMS) and the plasma wave instrument (PWI) [*Chappell et al., 1981; Shawhan et al., 1981*].

The RIMS consists of a retarding potential analyzer (RPA) followed by an ion mass spectrometer (IMS). The RPA voltage sweeps from 0 to 50 V, providing energy analysis, while the IMS distinguishes masses between 1 and 32 amu. For the events studied, the primary mode of the RIMS instrument is one which selects masses 1. 4, and 16 (H^+, He^+, and O^+). There are three detector assemblies available, one looking normal to the spin axis, with the other two looking parallel and antiparallel to the spin axis. Pitch angle distributions of the 0- to 50-eV ion flux are obtained from the detector looking radially outward from the spacecraft, normal to the spin axis. This detector has an angular resolution of approximately 20° in the spin plane. and 110° perpendicular to the spin plane. The RPA on the radial detector failed prior to the period used for this study, so no energy analysis is obtained from this detector. The spin axis detectors provide RPA analysis for ions moving parallel to the spin axis. These detectors are nominally looking perpendicular to the magnetic field at all times, with an angular resolution of 110°. One RPA/IMS cycle requires'/ s, and an angular distribution can be acquired in one spin of the satellite, i.e., in 6 s.

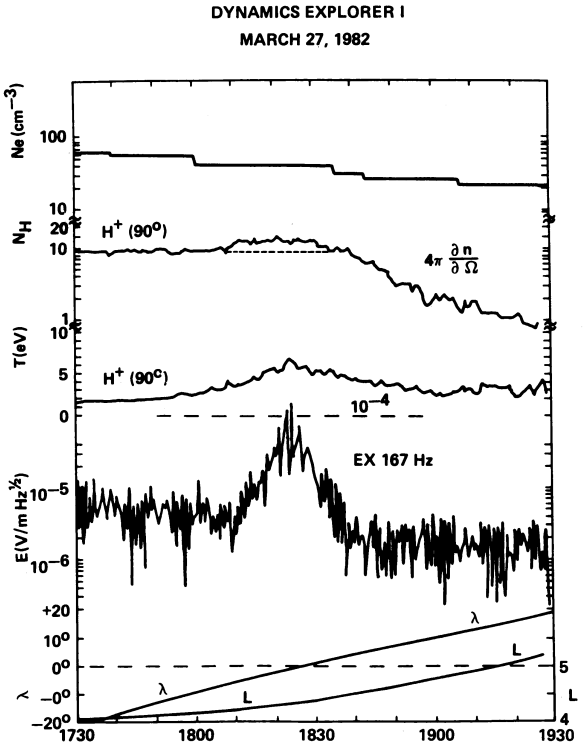

Fig. 2. Summary of plasma parameters. Total electron density, derived from PWI, is at the top. The ion distribution function is integrated to obtain the ion (H') density and temperature. Since the plasma is assumed to be isotropic when the distribution function is calculated, and integrated, the first moment is a pseudodensity, denoted $4\pi\partial n/\partial\Omega$ in these plots. The electric field strength at 167 Hz is next. The magnetic latitude (λ_m) and McIlwain "L" parameter are at the bottom, with scales on the left-hand and right-hand sides, respectively.

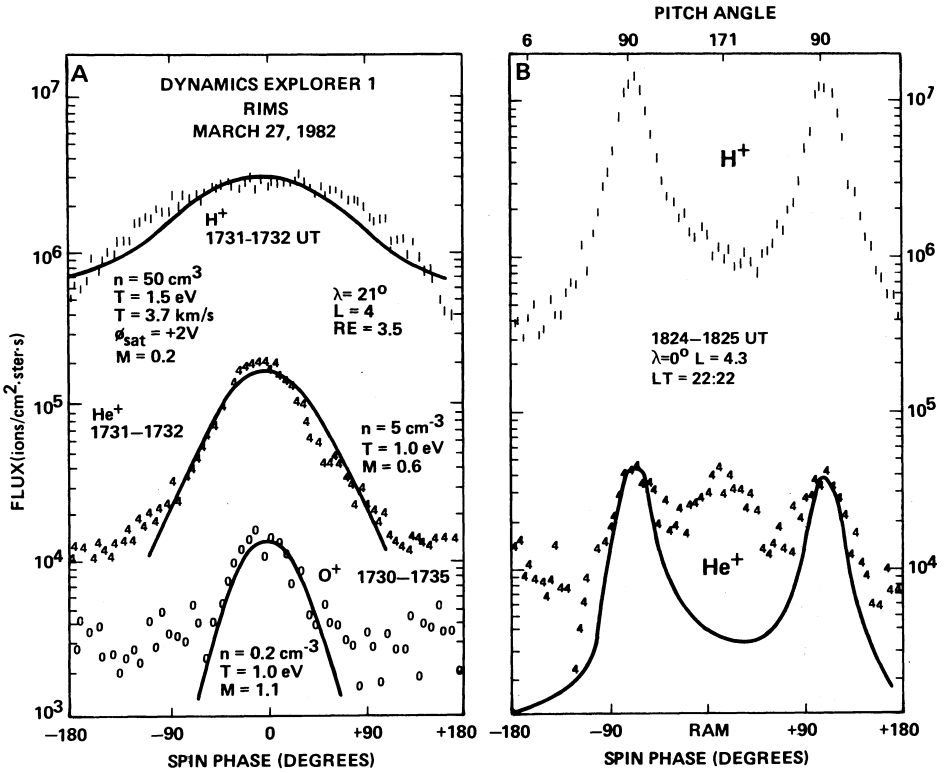

FIGURE 3

Fig. 3. (a) Spin curves for H^+, He^+ , and O^+ prior to the equator crossing. The data were fitted with the curves shown, and the resulting plasma parameters are noted beside each curve. (b) Spin curves for H' and He' at the magnetic equator. The line drawn through the He^+ data is the trace of the H^+ curve.

The PWI provides calibrated wave amplitude measurements from 1.8 Hz up to 409 kHz. using a low-frequency correlator (LFC) from 1.8 to 100 Hz. and step frequency receivers (SFR) from 104 Hz to 409 kHz. The LFC covers the 1.8- to 100-Hz frequency range in 8 logarithmic frequency steps, and the SFR covers the remaining range in 128 steps. A complete frequency sweep requires 32 s — just over five spins of the spacecraft. The receivers may be connected to the long electric antenna (Er), which is 200 m tip to tip, to the magnetic loop and search coil (B). and occasionally to the "short" spin axis antenna, 9 m tip to tip.

Day 86

The first example of equatorial plasma and wave measurements comes from March 27, 1982 (day 86). As in most of the examples shown in this paper, the magnetic activity was low at this time, with Kp = 1. The satellite orbit is illustrated in Figure 1. The orbit has been projected onto a plane at 2200 MLT. DE 1 is moving from south to north, beginning at L = 4 at 1730 UT. DE 1 crossed the magnetic equator at L = 4 at 1827 UT and reached L = 5.2 at 1930 UT. The satellite was in the outer plasmasphere. or plasmapause region throughout this period. The PWI data, described below, show the density ranging from 25 to 70 cm^{-3}.

The RIMS data are illustrated in Plate 1. Hydrogen data are displayed in the two top panels of the figure. The top panel is an RPA-time spectrogram for the (+Z) end head (90° pitch angle) data. The second panel is a spin-time spectrogram for the data taken by the radial detector at 0 V retarding potential. The center line is the ram direction which is nearly zero degrees pitch angle. The minimum pitch angle (near 0°) is indicated by the dashed white line running along the center of the spectrogram. The short-dashed line near the bottom of the panel indicates the spin phase for maximum pitch angle (nearly 180°). The fluxes are color coded, with dark blue representing low fluxes (10^5 ions/cm^2 sr s) and red representing high fluxes (10^7 ions/cm^2 sr s). The color bar on the left-hand side of the figure shows this scale. Note that each of the spectrograms in this paper has been scaled to emphasize the desired features, and the flux scale varies from figure to figure. The equatorially trapped plasma appears as the red regions in both panels. High fluxes, extending above 10 V on the RPA scale, and a flux peak at 90° pitch angle in the spin-time plot identify the warm anisotropic plasma trapped at the magnetic equator. Prior to this time, the plasma is a "ram" plasma, that is, primarily isotropic, and ordered by the spin phase (satellite velocity vector) instead of the pitch angle (magnetic field direction). After 1900 UT, faint traces of field-aligned ions become apparent, particularly in the helium (not shown). The presence of field-aligned ions indicates the satellite is leaving the plasmasphere, edging into the plasmasheet at L = 5. The latitudinal extent of the equatorially trapped plasma on this day (from λ = -15° to 15°) is one of the greatest found during the survey of 1982 data, particularly in this local time sector.

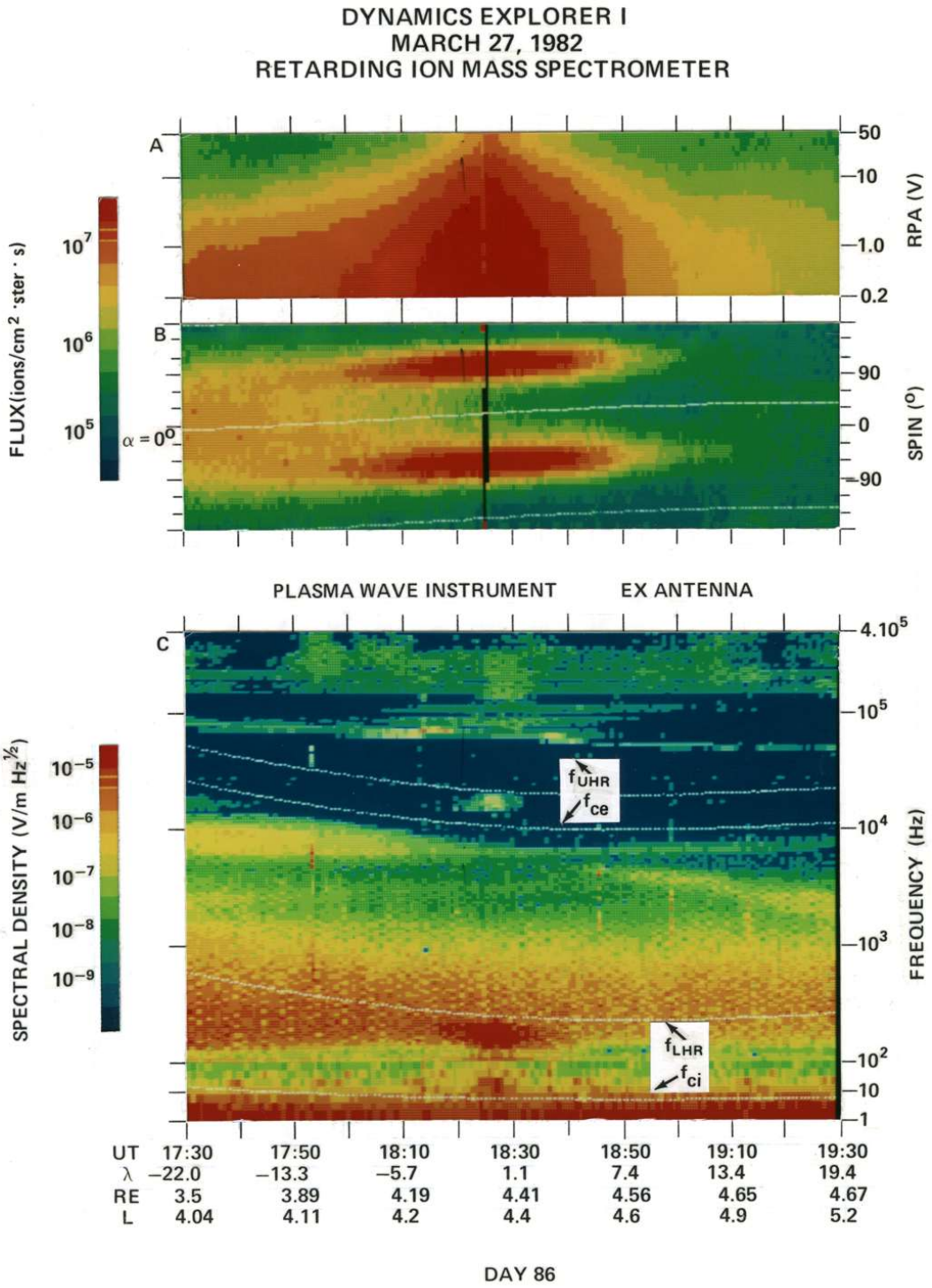

Plate 1. Day 86: (a) RPA-time spectrogram for H^+ measurements in the +Z ($\alpha = 90°$) detector. (b) Spin-time spectrogram for H^+, taken at 0 V RPA, from the radial detector. This detector responds to H^+ ions from 0 eV to several hundred electron volts. (c) Plasma wave data from the long electric antenna, perpendicular to the spin axis.

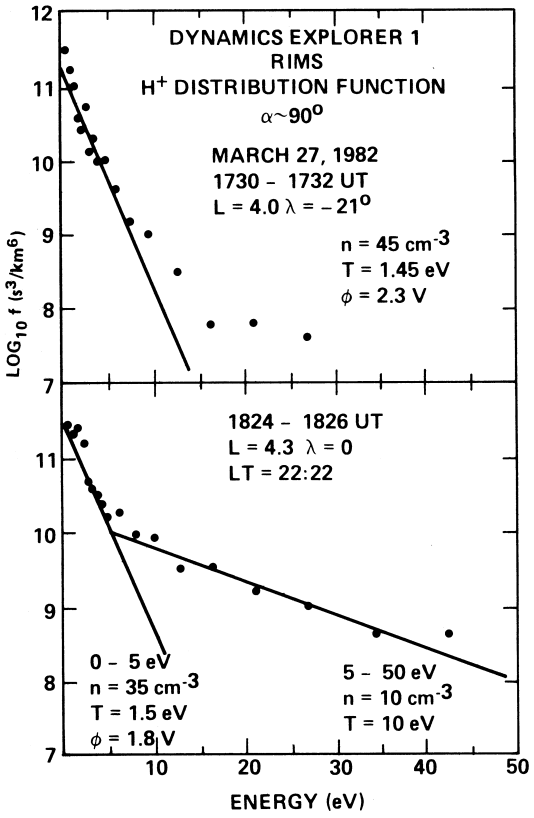

Fig. 4. Ion distribution functions for H'. (Top) Prior to the equator crossing. (Bottom) At the equator.

The plasma wave data are shown in the bottom panel of Plate 1. The electric component of the plasma waves, from the long (Ex) antenna, shows many of the features previously reported from this region of space. The upper hybrid resonance (UHR), used for plasma density determinations, begins near 100 kHz at 1730 UT, and drops slowly to 45 kHz at 1930 UT. It shows enhanced signal strength 5° to 10° from the equator, but drops in intensity at the equator. This latter effect is anomalous in the DE data set; normally the UHR intensifies at the equator. Below the UHR are the electron cyclotron frequency (f_{ce}), and the first harmonic, plotted as dashed white lines. At the equator (1827 UT), the 3/2 electron gyro-harmonic emission appears, as is generally found at the equator in the DE 1 data set. This is presumably the same intense emission studied by *Kurth et al.* [*1979*]. At frequencies below a kilohertz the geometric mean gyrofrequency $[(f_{ci}f_{ce})^{1/2}]$ is plotted. It drops from 500 to 200 Hz over this time period. The geometric mean gyro-frequency (f_{gmg}) is essentially equal to the proton-electron lower hybrid resonance (LHR) for the regions shown in this paper, and this line is therefore labeled as the LHR [*Stix, 1962*]. This estimate excludes the effects of heavier ions on the LHR, i.e., a lowering of the frequency. This exclusion is generally a small effect in our data — a typical 10% helium component will only lower the LHR by 5%. The intense signal (red spot) below the LHR, at the equator, is the equatorial noise. Below this signal is the hydrogen gyrofrequency, plotted as a dotted white line, which remains near 10 Hz across the plot. The red band below the hydrogen gyrofrequency is primarily due to solar array noise.

Figure 2 shows the variation in the total plasma density (UHR), and the density and temperature moments for the observed hydrogen distributions. The total density drops through this period. The lack of evidence for a substantial density increase at the equator provides an answer to one question raised by previous measurements. Though the equatorially trapped plasma represents a tremendous increase in flux for particle detectors, it is not primarily an increase in the total plasma density. The RPA data from the end head (90° pitch angle) were converted to distribution functions (Figure 4. described below), and then integrated to obtain the first and third moments, i.e., density and kinetic temperature. This procedure allows us to characterize the equatorially trapped plasma, even though it does not show a Maxwellian distribution. Because of the positive spacecraft potential found in such regions (+1 to +4 V on the end head), the cold background plasma is not well measured by this detector. The density and temperature obtained from the end head data are therefore the parameters for the warm component only. These are the parameters plotted below the total density in Figure 2. Note that both the density and the temperature of the warm plasma peak at the equator. Next, the electric field strength near the spectral peak of the equatorial noise (167 Hz) is plotted to provide a measure of the equatorial noise intensity. Fluctuation in the electric field amplitude is due to spin modulation and beating between the spin period and sampling period.

Figure 3 shows the spin curves for hydrogen and helium prior to (Figure 3a) and at (Figure 3b) the equator crossing. The off-equator data are fitted with a rammed. isotropic Maxwellian distribution, using an algorithm developed by *Comfort et al.* [*1985*]. Discrepancies between the model spin curves and the data indicate the beginnings of the development of anisotropic distributions. In particular, the shapes of these curves are consistent with a heat flux away from the equator [*Biddle et al., 1985*]. At the equator, both species exhibit trapped signatures, i.e., peaks at 90° pitch angle. The hydrogen flux is two orders of magnitude higher than the helium flux. The hydrogen spin curve has been traced and superimposed on the He' data. The hydrogen and helium spin curves have similar shapes, except for what appears to be a field-aligned helium flux near 0° spin phase. The shape of the H' spin curve is that expected from a bi-Maxwellian distribution, with $kT_{\parallel} = 0.5$ eV, $kT_{\perp} = 5$ eV, and a spacecraft potential of +1 to +2 V. This is not the only type of plasma distribution which will produce the observed spin curve, but it is a good candidate. These data do not address the question of whether the core or the tail of the distribution is heated, since the core of the plasma population is obscured by the heated plasma. The higher hydrogen flux is in contrast to the preferential heating of helium inferred from GEOS 1 and 2 observations near the equator, in association with ion cyclotron waves below the hydrogen cyclotron frequency [*Young et al., 1981*].

Figure 4 shows the RPA data from the end head, converted into distribution function form. The pre-equator data are fitted over the 0- to 10-eV energy range with a

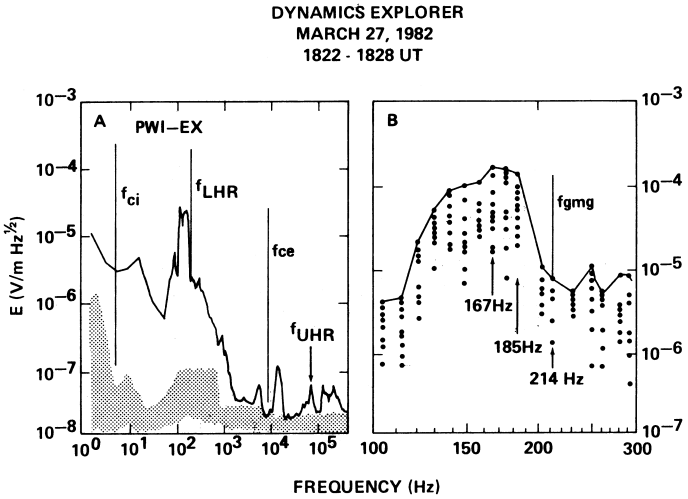

Fig. 5. Electric field spectrum at the equator. (a) Spin-averaged spectrum. The dotted pattern is the noise level. (b) all data points plotted.

Maxwellian with parameters noted on the figure. The moment calculation used in Figure 2, provides a higher temperature (1.8 eV) because of the higher-energy tail, and a lower density (9 cm^{-3}) because there is no correction for satellite potential in the moment integration. Superimposed on the plot of equatorial data are two Maxwellian segments indicating the low-temperature component seen away from the equator, and the hot tail. The plasma parameters found here suggest that the core of the plasma population has not been substantially changed. and the equatorially trapped plasma is just the tail of the distribution in this event. The moments of the distribution function at the equator are n = 12.4 cm^{-3}, T = 6.6 eV for hydrogen. Moment calculations for the helium data give a similar temperature (5 eV) and a density of 0.6 cm^{-3}. The high hydrogen to helium ratio is similar to the result obtained by *Quinn and Johnson* [*1982*] at higher energies. The hydrogen to helium ratio for the heated plasma is similar to the 10:1 ratio found by RIMS for the cold plasma away from the equator.

Figure 5 shows the electric field spectral density at the magnetic equator. Six minutes of data (and hence many spins) have been averaged, showing the equatorial noise between 100 and 200 Hz, a 3/2 f« emission feature, and the UHR. Figure 5b shows an expanded spectrum from 100 to 300 Hz. and shows all the measurements for the 6-min interval. The fluctuations are primarily due to the spin modulation of the signal. The cutoff between 185 and 204 Hz is consistent with a 10% He^+ (and 0.4% O^+) ion composition, and a resulting cold plasma lower hybrid resonance frequency of 204 Hz. The equatorial noise power flux, integrated over the bandwidth, is 10^{-7} to 10^{-8} W/m^2. The magnetic component (not shown) shows a similar spectra from 100 to 300 Hz, with an amplitude of 10^{-2} γ.

This example has illustrated the major features of the equatorially trapped plasma as viewed by RIMS, and the equatorial noise which is frequently associated with the warm plasma. The heated plasma is found in the plasmapause region, where the ambient plasma density is in the 10-100 cm -3 range. The trapped plasma is primarily H^+, with about a 10% He^+ concentration. Although there is a tremendous enhancement in flux, there is not an enhancement in total plasma density.

Day 52

One of the most unusual observations of trapped plasma was made on February 21. 1982 (day 52). The magnetic activity is high, with Kp = 3+ . During the previous 24-hour period. Kp fluctuated between 2 and 5. providing the most active period illustrated in this article. The satellite is in the plasmasphere, at local midnight. and is in eclipse. Because the satellite is in eclipse, the potential is less positive than it would normally be. and the core or cold plasma measurement is enhanced [*Olsen et al., 1985*]. The orbit for this event is shown in Figure 6. DE 1 moves from L = 3.5 to 4.3, crossing the equator at L = 4 at 1920 UT. Between 1945 (L = 4.5) and 1950 UT (L = 4.6) the satellite encounters the plasmapause. The inferred heating region is shown as a shaded region which is symmetric about the equator, and narrows with radial distance. Plate 2 summarizes the RIMS H^+ and He^+ data. Unfortunately, the PWI was turned off for much of this period, including the equator crossing. The RIMS data show sharp transitions from ram, isotropic plasma to the equatorially trapped distribution at 1905 and back to isotropic plasma at 1927 UT. The peak in ion flux occurs a few minutes before the nominal equator crossing, indicating either an error in the determination of magnetic latitude of 1° to 2°, or a radial variation in the heated plasma. The helium data reveal similar behavior, with the background and heated helium populations both at about 10% of the hydrogen density. Little or no oxygen is present, in cold or heated form.

The plasma wave data show an UHR near 100 kHz over most of this period, indicating a density near 100 cm^{-3}. The transition from equatorially trapped to isotropic plasma at 1927 occurs just after the PWI is switched on again. The latter transition corresponds to an increase in density as the satellite leaves the equator, from 80 cm^{-3} to 190 cm^{-3}. Whatever equatorial noise signature was present at the equator has faded by the time the PWI is switched on.

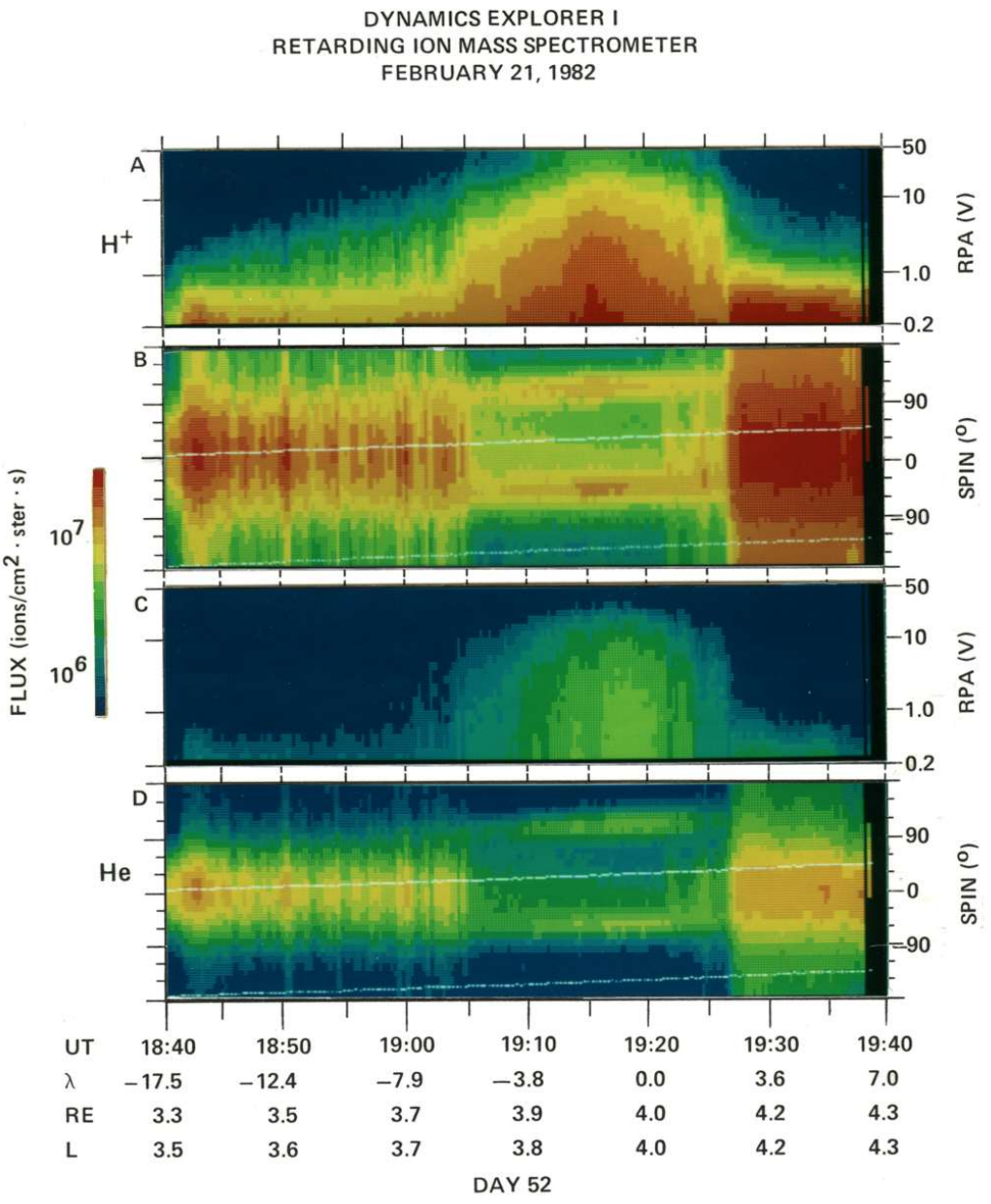

Plate 2. Day 52: (a) RPA-time spectrogram for H^+ from the -Z ($\alpha = 90°$) detector. (b) Spin-time spectrogram for H^+, radial detector, 0 V RPA. (c) RPA-time spectrogram for He^+. (d) Spin-time spectrogram for He^+.

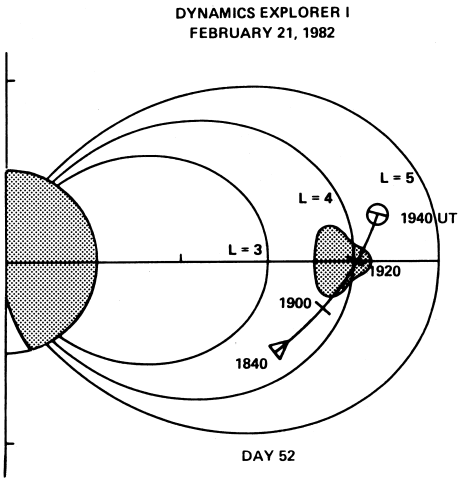

Fig. 6. Orbit plot for February 21. 1982.

Both the RIMS and PWI data show a relatively rapid fluctuation in the ion flux and UHR, respectively, prior to the equator crossing. This can be considered as primarily temporal (i.e. not a result of satellite motion), or primarily spatial (i.e. the satellite is flying through quasi-static structures). In the latter case, it may either be due to radial (L shell), latitudinal, or local time variations in the ambient plasma structure. Our current explanation of these fluctuations and a number of similar observations is that there is a latitudinal structure, established by the plasmasphere filling process. Note that this structure does not persist through the equator, as though the equator represents a barrier to interhemisphere communication.

Figure 7 summarizes the reduced plasma parameters for this set of observations. The difference between the electron and ion densities, derived from the PWI and RIMS, respectively, can be explained by a +1-V potential on the detector. The ion density is constant through the equator, while the temperature increases by an order of magnitude. Both the ion and electron density increase sharply at the high-latitude boundary to the region of heated plasma at 1927 UT. Note that the density is higher above the equator than it was at lower L shells below the equator.

Figures 8a. 8b, and 8c contrast the spin curves prior to, during, and after the equator crossing, respectively. The ram distributions are again fitted with rammed, Maxwellian plasma distributions. These fits were done assuming zero satellite potential, which probably results in a slight underestimate for the plasma density, particularly in Figure 8a, 1900—1902 UT. The hydrogen spin curves at the equator appear to be a combination of isotropic plasma and trapped plasma. In particular, the curvature near 0° spin phase indicates the angular distribution is not so much a bi-Maxwellian (which results in curves like those in Figure 3) as the sum of a cold and warm population. The isotropic hydrogen component has a density which is less than 10% of the off-equator values. This low percentage suggests that the bulk of the cold isotropic plasma has been converted into the heated, equatorially trapped plasma, and that in this case the heated plasma is not just the heated tail of the core plasma.

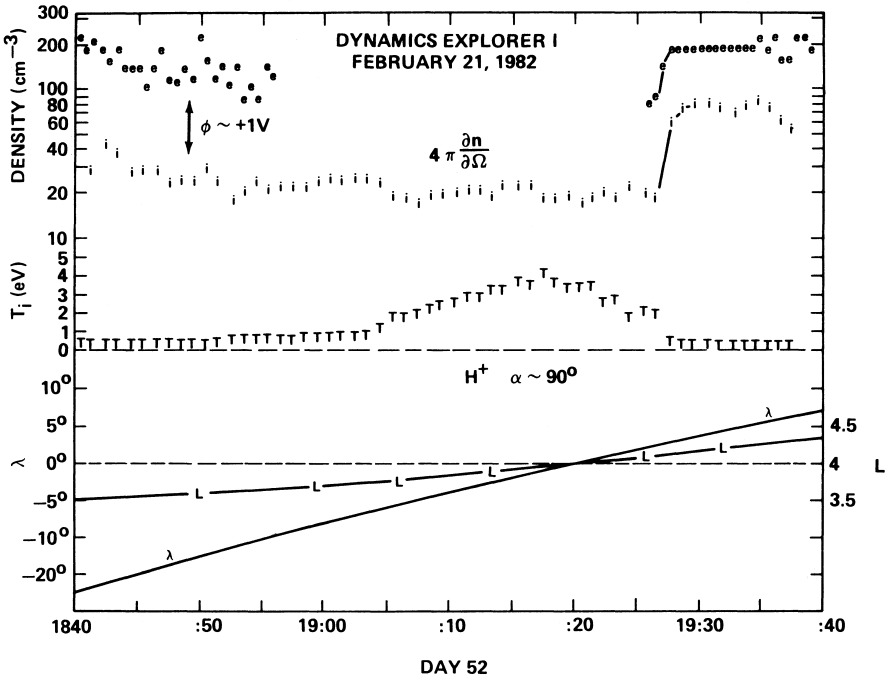

Fig. 7. Summary of plasma parameters with total electron density (e). ion (H^+) density (i), ion (H^+) temperature (T), magnetic latitude, and L.

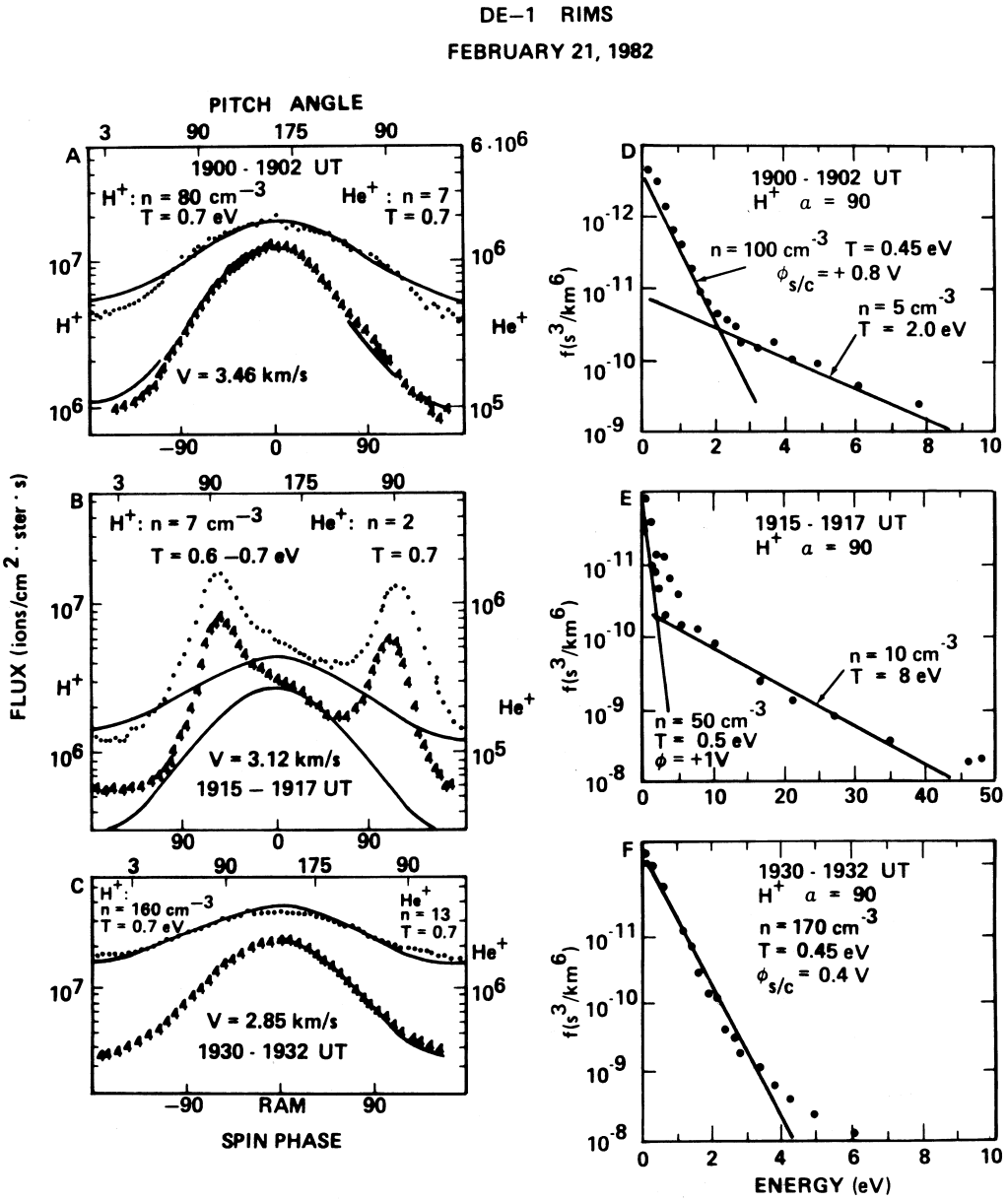

Fig. 8. (a) Spin curves for H^+ (circles) and He^+ (4's) prior to the equator crossing, with fits. (b) Spin curves at the equator, with lines drawn for the same temperatures found in Figures 8a and 8c at reduced densities. (c) Spin curves after the equator crossing. (d) H^+ distribution function for the period shown in Figure 8a. (e) H^+ distribution function for the period shown in Figure 8b. Note the change in energy scale as compared to Figures 8d and 8f. (f) H^+ distribution function for period shown in Figure 8c.

RPA data from the end head are again converted into distribution functions, as shown in Figure 8, with Maxwellian segments plotted over the data. Prior to and after the equator crossing, cold dense plasma is found. The temperatures are lower than those used in the spin curve fits, reflecting the influence of the warm tail on the spin curves. A fit for the cold plasma is superimposed on the 0- to 10-eV energy range of Figure 8e, but it is not clear if the scattered data points at low energy warrant such a fit, since the differentiation process can produce a few random points at low energy (we are differencing large numbers and dividing by increasingly small ones at low energies). (Note that the energy scale for Figure 8e is higher than that used for Figures 8d and 8f.) The 5- to 50-eV data indicate a density of 10 cm^{-3}, and a temperature of 8 eV — this is the heated plasma. The moments of the distribution functions away from the equator (as plotted in Figure 7) are similar to the fitted values, except for the effect of the 0.5- to I.0-V satellite potential. At the equator, the moments of the distribution function are n = 22 cm^{-3}, T = 3.6 eV.

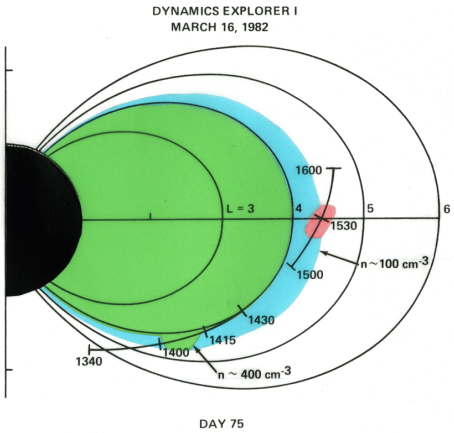

Fig. 9. Orbit plot for March 16. 1982. The inner shaded region is the plasmasphere, which apparently extends beyond L = 4 at high latitudes (1400-1415). The plasmapause region is indicated with lighter shading, and the region of equatorially trapped plasma by the darker dot pattern.

Day 75

One of the implications of the previous example is that there are relatively sharp spatial (latitudinal) boundaries delimiting the region of equatorially trapped plasma. particularly in magnetic latitude. This idea is extended by the next example from March 16. 1982 (day 75). Kp is 1 and was between 1 and 2 for the previous 24 hours. Figure 9 shows two orbital segments for this day. The satellite crosses the plasmapause twice over this period. first at 1402 UT. and again near 1510 UT. both times at L = 4.2. This is the 100 cm^{-3} boundary, and is quite sharp at 1400 UT (λ_m = -37°). One peculiarity of the plasmapause structure found on this day is that the density shows a local maximum from 1400 to 1415 UT (L = 4.3 to 4.0, λ_m = -37° to -27°). The density maximum does not appear in the later equatorial crossing of the same L shells. Based on these boundary crossings, the inner shaded region in Figure 9 is used to indicate the cold, "inner" plasmasphere, with a 400 cm^{-3} boundary at L = 4 at most latitudes, but a bulge or dimple which the satellite encounters between 1400 and 1415 UT. Unfortunately, there is a data gap from 1430 to 1500 UT. The plasma density is the same at 1500 UT as at 1430 UT, so we can only speculate that it was constant over this time period. Further information on the plasmapause location can be obtained from ISEE 1, which encounters the plasmapause (inbound) at 1742 UT, 0642 LT, λ_m = -38°, 3.15 RE, L = 5.3. Outbound, ISEE 1 crosses the 100 cm -3 boundary at 1947 UT, 2148 LT, 4.0 RE, λ_m = 13°, and L = 4.2. This combination of boundary crossings brackets the DE measurements near local midnight (2300 LT). A 100 cm^{-3} boundary is indicated by the light shaded region from L = 4 to 4.2. The region of heated plasma is indicated by the small dark ellipse at the equator.

Plate 3 shows the RIMS data for the equator crossing. The helium fluxes have been enhanced by two orders of magnitude to bring them onto the hydrogen flux scale. A plasmapause signature is visible near 1510 UT. In the RPA data (Plates 3a and 3c), the red regions in the lower left-hand corners show the fading of the cold plasmasphere plasma. In the He^+ spin-time spectrogram (Plate 3d), evidence of field-aligned plasma appears, primarily in the 180° pitch angle (-180° spin phase) data. The hydrogen spin-time spectrogram (Plate 3b) shows a distribution peaked at 90° pitch angle, as one now expects at the equator. Also, the hydrogen RPA data (Plate 3a) show a substantial increase in flux at the equator. The helium RPA data show a minimum in this region. with distinct boundaries at 1520 UT and 1535 UT (λ_m = ±3°) as though helium ions are excluded from the equator. The intensity of the field-aligned He^+ flux also decreases over this period, with a particularly noticeable increase upon leaving this region at 1537.

Plate 4 shows the PWI data for this period. The short spin axis antenna is being used at this time. The data from this antenna are noisier than those shown in the previous examples. and are only used to identify the UHR. The UHR and 3/2 f_{ce} signals intensify near the equator, and a brief signal is found just below the LHR at 1525 UT. The broad spectrum previously associated with the ion Bernstein modes is not seen here, and the emission below the LHR at 1525 UT may not be the "equatorial noise" normally found with the equatorially trapped plasma, but rather a lower hybrid resonance emission.

Figure 10 shows the reduced plasma parameters for this period. The format of Figure 10 is similar to that used in Figure 7. The UHR derived total electron density is plotted at the top. Much of the fluctuation following 1520 UT is probably a fluctuation between enhancements of the sixth and seventh (n + ½) electron gyroharmonics which contribute to the UHR signal. Next the hydrogen and helium densities, as obtained from the RPA data. are plotted. The helium values have been multiplied by 10 to compress the plot. The hydrogen and helium densities are highest at 1500 UT. as the satellite is leaving the plasmasphere. Again the difference

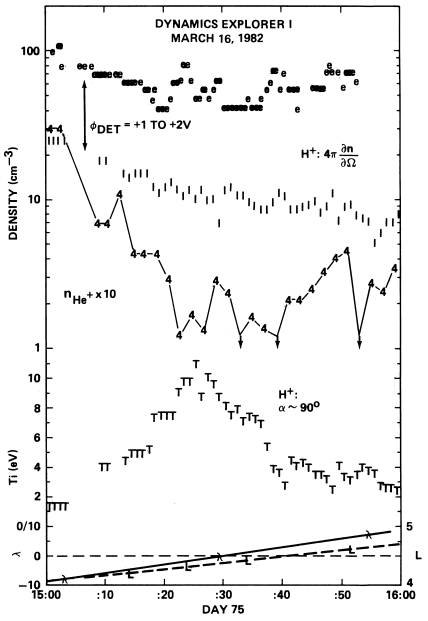

Fig. 10. Summary plot for March 16, 1982. Total electron density, hydrogen density, helium density (x10), hydrogen temperature, magnetic latitude, and L.

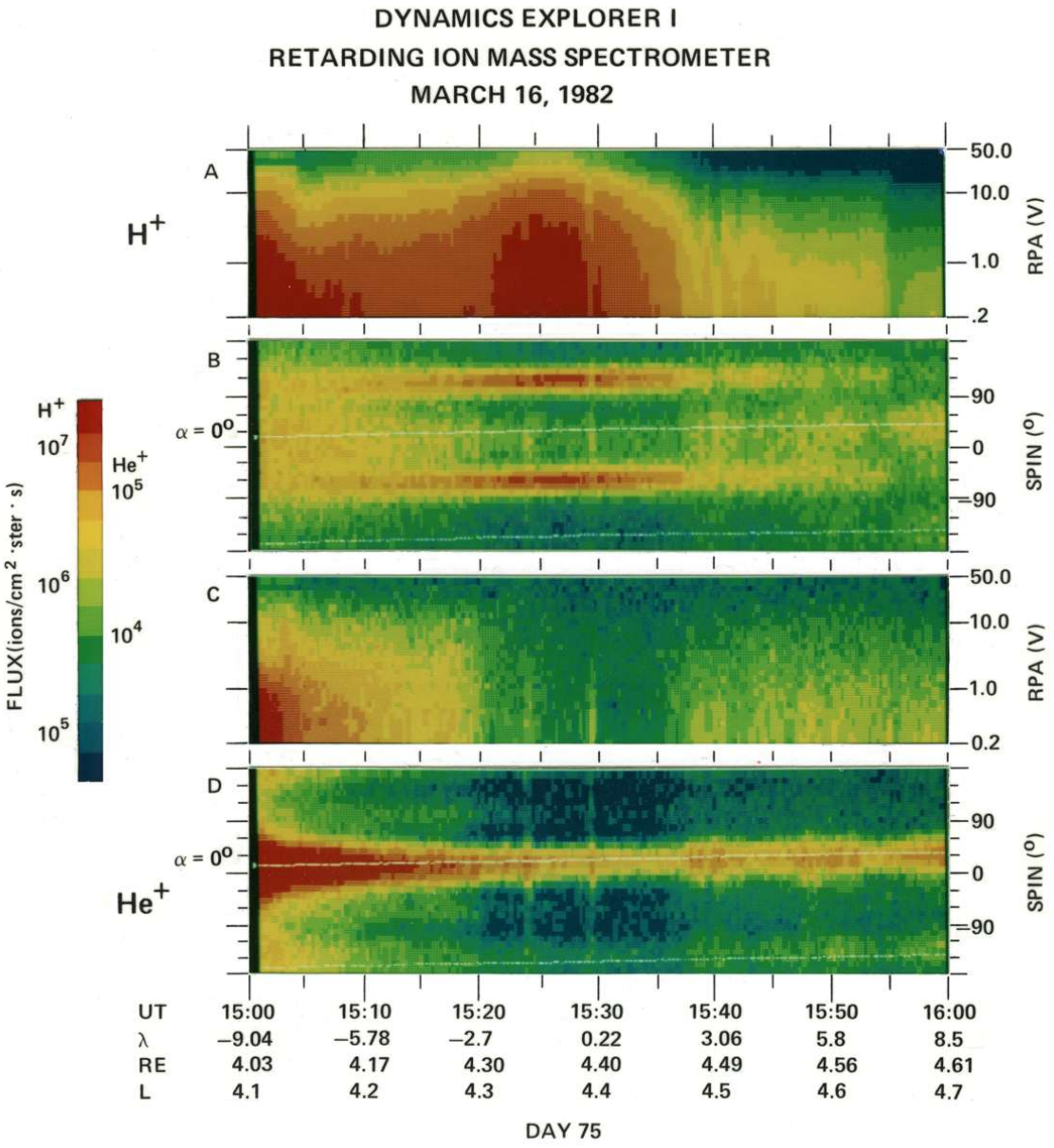

Plate 3. Day 75: (a) RPA-time spectrogram for H'. (b) Spin-time spectrogram for H'. (c) RPA-time spectrogram for He. (d) Spin-time spectrogram for He.

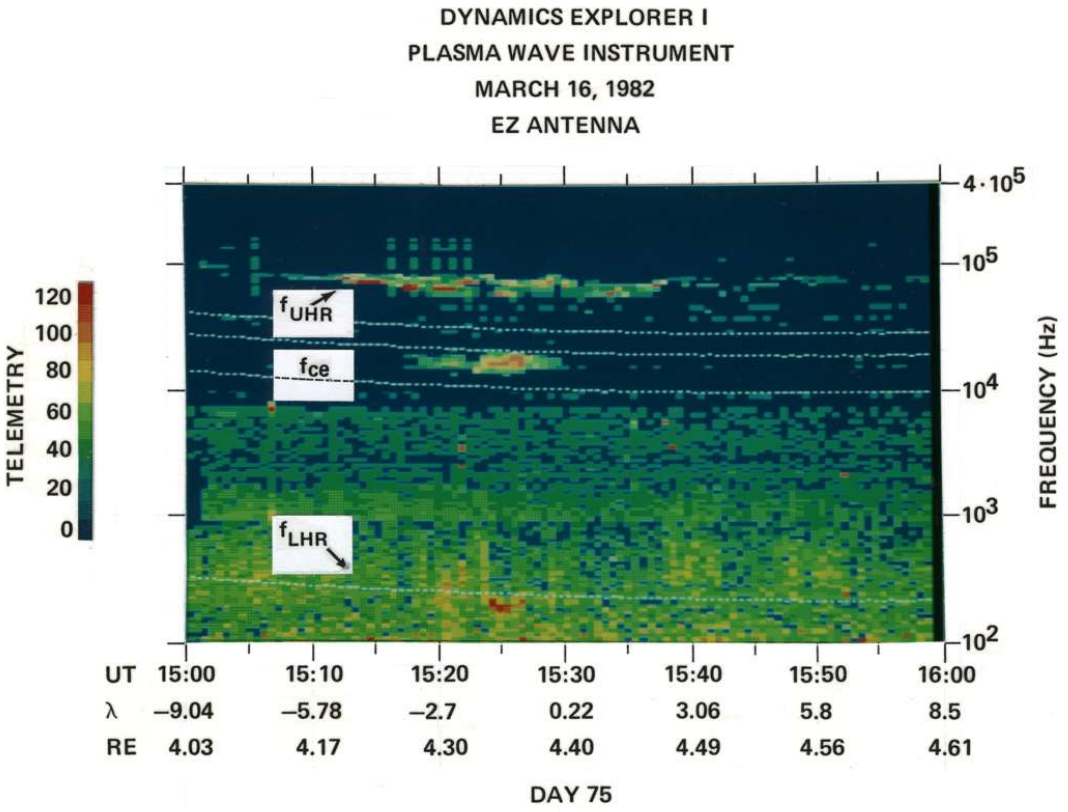

Plate 4. Plasma wave data from the spin axis electric field antenna, day 75. Raw telemetry ranges from 0 to 256, with only the bottom half of that range used for this plot. The telemetry is the uncalibrated, logarithmically compressed antenna voltage.

between the proton and electron density from 1500 to 1510 is primarily due to a +1- to +2-V detector potential. The warm proton density is then constant through the equator. while the helium density shows a minimum, as implied by the spectrogram. The ion density from 1520 to 1600 is less than the electron density because most of the core plasma is hidden by the increasingly positive detector potential [*Olsen et al., 1985*]. The proton temperature, plotted below the density profiles, shows an order of magnitude increase at the equator.

These data show that (1) in this case, only protons are heated, (2) the thermal helium is excluded from the equatorial region, and (3) only a small wave signal near the LHR is found. We infer that the heating of the plasma at the equator increases the plasma potential, which causes a decrease in the ion density (exp(-eΦ/kT)). This positive potential causes the field-aligned He^+ flux to lose kinetic energy as it enters this region. The reduced flow velocity results in a lower flux. The latitudinal extent of the LHR-related emission does not match that of the heated ions.

A similar data set has recently been published as part of a study of Pc 5 observations by *Engebretson et al.* [*1986*]. In Plates 1 and 2 of that paper, equatorially trapped H^+ is found in the plasma sheet, in a region of field-aligned H^+, He^+ , and O^+. In that example, the field-aligned H^+ persists through the equator, and the two heavier ions remain field-aligned. A similar event is shown by *Decreau et al.* [*1986*], in Plates lb and 1c. The satellite is in a region of field-aligned plasma (i.e., the plasmapause), with H^+ exhibiting both trapped and field-aligned components at the equator.

The examples shown so far have illustrated the ideas that the equatorially trapped plasmas are primarily hydrogen, and that the enhanced fluxes are the result of a temperature increase, not a density increase. Indeed, the equatorial region may represent a local minimum in density. The conversion from isotropic to equatorially trapped plasma has been shown in several cases, and indications of an apparent transition from field-aligned to trapped plasma were found in the last example. In the next case, indications of a density minimum are found, along with suggestions that the field-aligned ions are either converted into the trapped plasma at a sharp boundary, or are being reflected at a potential structure near the equator.

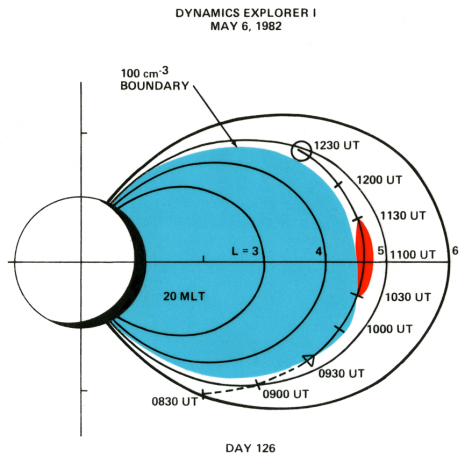

Fig. 11. Orbit plot for May 6, 1982. The plasmasphere and equator region are shaded.

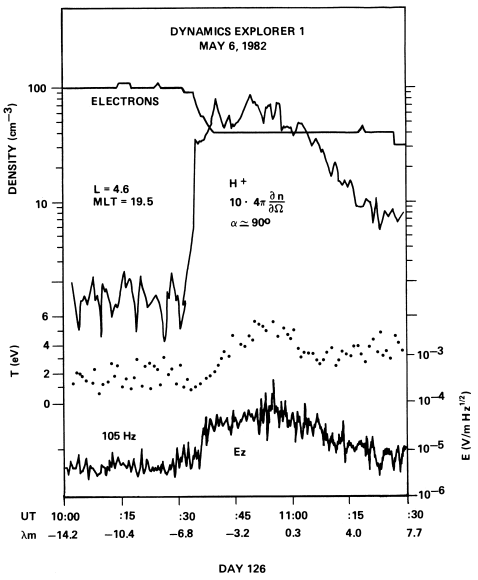

Fig. 12. Summary plot for May 6, 1982, 1000 to 1130 UT.

Day 126—1100 UT

Two orbits from May 6, 1982 (day 126), are shown. The orbit which provided an equator crossing at 1100 UT is illustrated first, in Figure 11. The satellite crosses the plasmapause at high and then low latitudes. The high-latitude crossing is at 0930 UT. The satellite is at L = 4.7, λ_m = -22°. As the satellite approaches the equator, it again crosses the density gradient, but at a lower L value. The low-latitude gradient is found at L = 4.6, λ_m = -6°. This has been interpreted as shown by the large shaded region in Figure 11, indicating a plasmasphere that is dimpled near the equator, and bulges outward between -7° and -22° magnetic latitude. The region for heated plasma measurements is indicated with the darker shaded region extending along the satellite orbit from 1030 to 1130 UT. The satellite is at local dusk (1936 LT). *Kp* was 2- at this time, was between 2- and 2+ for the previous 12 hours, and was 3 for the 12 hours before that.

Plate 5 shows the RIMS and PWI data for this period. The RIMS spin-time spectrogram for hydrogen shows a field-aligned distribution which abruptly becomes a "pancake" distribution at 1035 UT. The helium data are similar to the hydrogen. with fluxes 1 to 2 orders of magnitude lower than the hydrogen flux. The PWI data show a drop in the UHR at 1035 UT and the appearance of the equatorial noise. There is an intensification of the UHR, the appearance of continuum radiation, and at least the first four of the (n + ½) electron gyroharmonic emissions at the equator.

Figure 12 shows the reduced plasma parameters for this day. The top curve shows the decrease in density from 100 cm^{-3} to 40 cm^{-3} from 1033 to 1038 UT. The density of the warm hydrogen (the core, or cold component. is again "hidden" by the positive detector potential, particularly in the moment calculation) shows a sharp rise, reflecting the

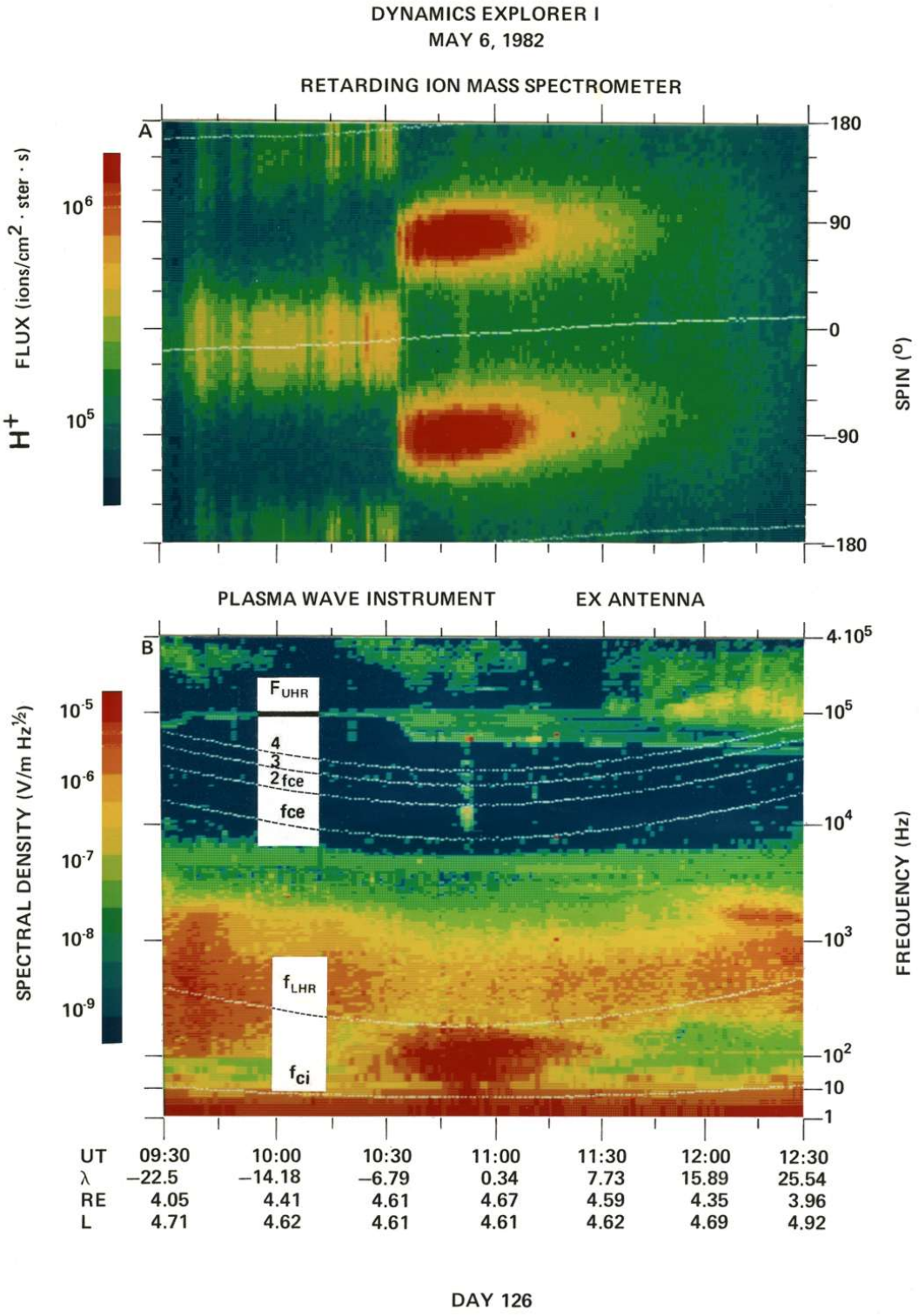

Plate 5. Day 126: (a) Spin-time spectrogram for H. (b) Plasma wave data from the long electric antenna.

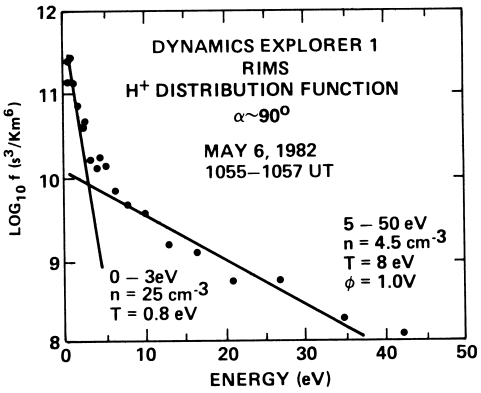

Fig. 13. H^+ distribution function at the magnetic equator.

increase in the plasma temperature. as shown in the next curve of the figure. At the bottom of the figure, the 105-Hz signal from the spin axis antenna indicates a similar abrupt transition in the equatorial noise. (The signal in this antenna is near background from 1000 to 1030 UT.) The spin curves for H^+ and He^+ (not shown) are similar to those shown in Figure 3b, for H^+, with the H^+ flux about 50 times the He' flux. Such curves indicate a bi-Maxwellian distribution as noted previously. Figure 13 shows the hydrogen distribution function, with a low-energy component inferred from 0 to 3 eV, characterized by a 0.8-eV temperature, a density of 25 cm^{-3}, and satellite potential of 1 V. The higher-energy data (5–50 eV) can be fitted with a 4.5 cm^{-3}, 8-eV Maxwellian segment.

Figure 14 shows the electric field spectrum. Ten minutes of data were used to reduce the effects of spin modulation of the highly polarized signal, and the peak values are plotted here. Most of the wave power is in the 10- to 100-Hz frequency range. The spectrum is again bounded by the lower hybrid frequency (or geometric mean gyrofrequency). The nature of the spectra below 100 Hz is obscured by the relative lack of resolution there, with only eight channels in the 1- to 100-Hz range.

The sharp boundary in density and plasma characteristics at 1035 UT (λ_m = -7°) can be interpreted as a boundary in radial distance, with a simple drop in density with altitude. The corresponding increase in positive satellite potential could then prevent the observation of the low-energy field-aligned flows. One problem with this interpretation is that RIMS normally observes field-aligned ion distributions throughout the plasmapause and plasma sheet. The energies of these flows typically increase with L, rather than disappear [*Olsen. 1982*]. A second possibility is that these are variations in latitude, resulting from heating and a subsequent increase in plasma potential near the equator. The field-aligned ions seen before 1030 UT approach the equator from behind the satellite, "bounce" off the electrostatic potential barrier, and are then seen returning from the equator (at 0° spin phase). The (apparently) larger flux at 0° spin phase reflects the low energy of the field-aligned ions, and the effect of the satellite velocity, which must be comparable to the field-aligned flow velocity (a few kilometers per second). As in the first example shown, there is a strong correlation between the equatorial noise and equatorially trapped plasma.

Day 126—Hour 3

The second of the events from May 6. 1982, provides similar plasma measurements to those shown first in this paper, from March 27. The satellite moves from the plasmasphere, and a region of isotropic plasma. into the equatorially trapped distributions. This orbit also features a high-latitude plasmapause crossing, and a fortuitous overlap with ISEE 1. The satellite orbits are illustrated in Figure 15. DE l crosses the equator at L = 4.3 at 0300 UT, 2000 LT. DE 1 had crossed this L shell earlier in the same orbit at 01223, at -42° λ_m, and 2000 LT. ISEE 1 is outbound from perigee at this time, crossing L = 4.3 at 0018 UT, at 24° λ_m at 1800 LT. This is nominally the plasmapause position at high latitudes, as determined by both satellites.

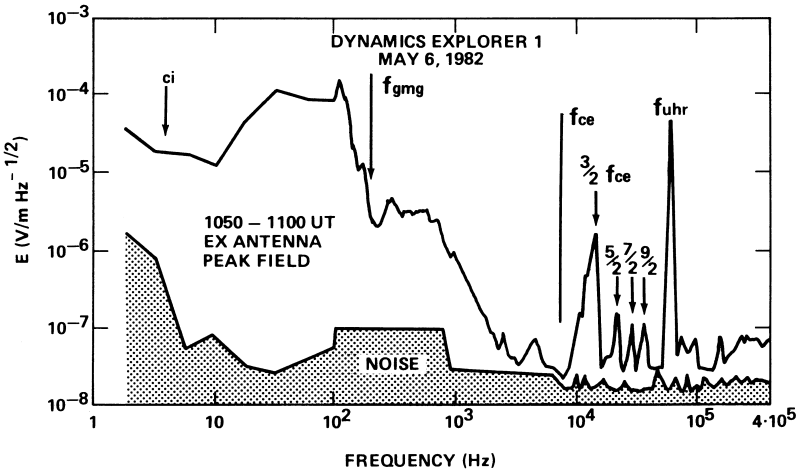

Fig. 14. Electric field spectrum at the magnetic equator.

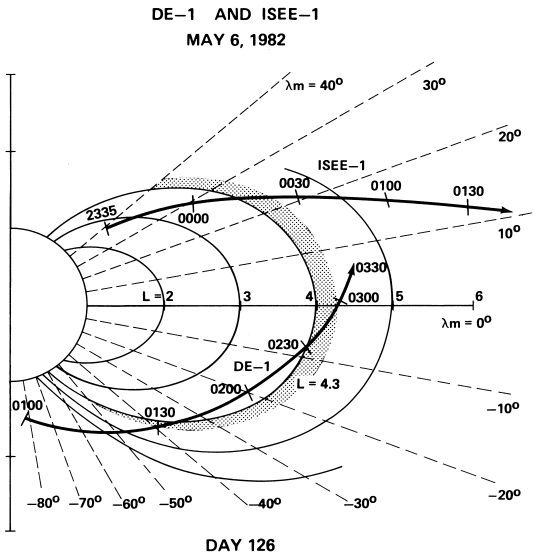

Fig. 15. Orbit plot for DE 1 and ISEE 1.

The DE 1 data for this orbit are summarized in Plate 6. The hydrogen data are shown in the top two panels. The RPA data are shown in Plate 6a, and the H angular distributions are shown in Plate 6b. A plasmapause signature is found in the RPA data between 0120 and 0130 UT, where a warm plasma is found, as the satellite rises from perigee. The satellite enters the plasmasphere, and remains there until reaching the magnetic equator. The RPA data show low energies in the plasmasphere away from the equator, then high fluxes and energies near the equator (the red region on the right-hand portion of Plate 6a). The spin distributions show rammed, isotropic plasma from 0130 to 0230, again indicating the satellite is in the plasmasphere. The three narrow vertical stripes at 0141, 0148, and 0157 are similar to the narrowly confined latitudinal structure inferred from the February 21 data (Plate 2). These are primarily density enhancements, not temperature increases. At the equator, the angular distributions change from isotropic to equatorially trapped. The plasma wave data show the UHR is monotonically dropping, demonstrating that the density is dropping, even as the flux is increasing. This must be due to a temperature increase. The He^+ data (not shown) show the cold plasma is about 10% He^+, while the heated plasma is about 1% He^+. The lower-frequency portion of the PWI data (Plate 6c) does not show a clear equatorial noise signature on this day, but there may be a signal near the LHR at the equator, and a lower-frequency feature prior to the equator crossing.

The reduced plasma parameters for the equator segment are shown in Figure 16. The total plasma density drops monotonically over this period, while the warm ion density and temperature peak just prior to crossing the equator. The satellite is moving out through the plasmapause at the same time, so radial effects are being superimposed on the latitudinal profile. The drop in flux (or n and T) with latitude is quite rapid outside the plasmasphere, where the total density is 20 cm^{-3}.

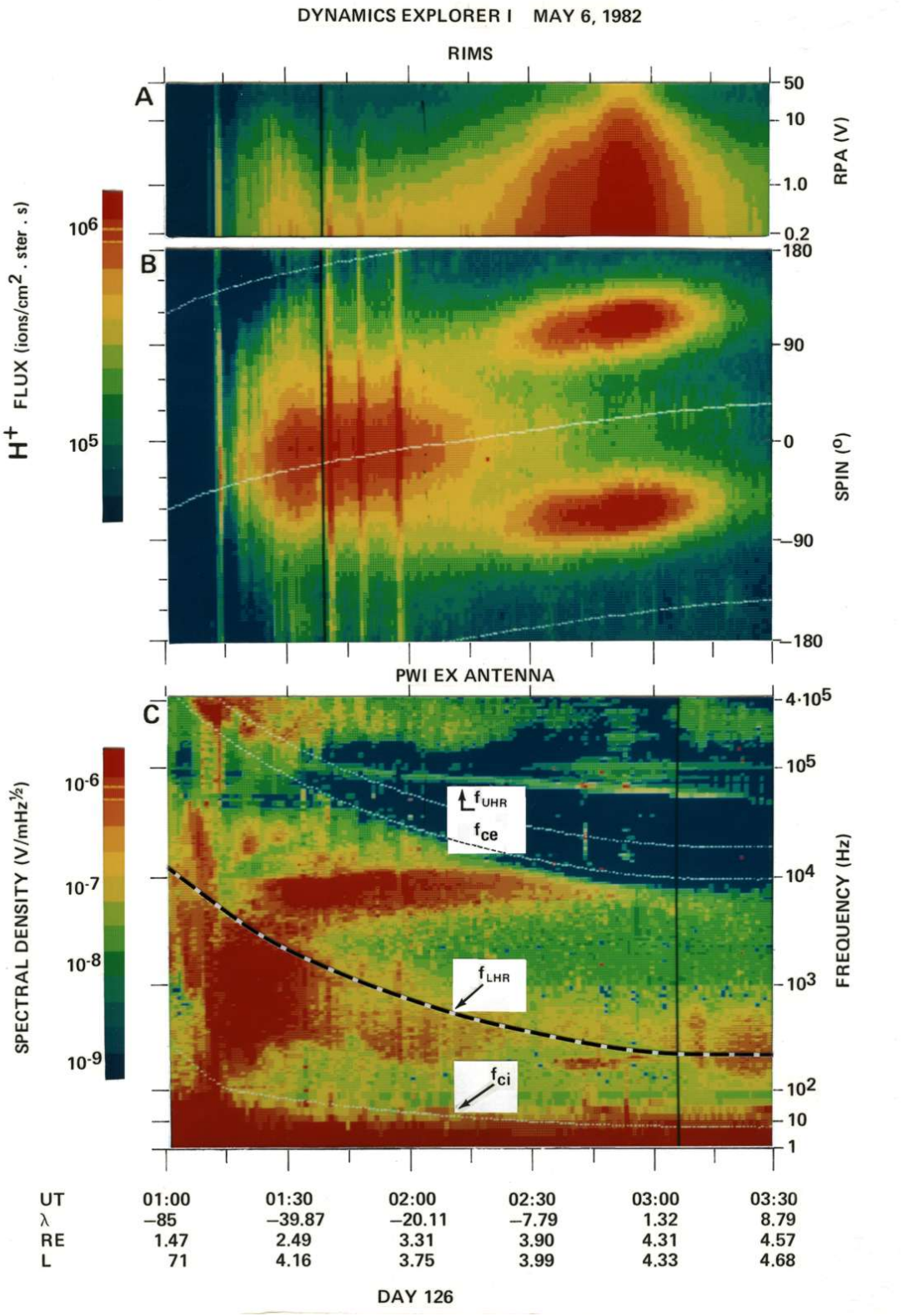

Plate 6. Day 126: (a) RPA-time spectrogram for H . (b) Spin-time spectrogram for H (c) Plasma wave data from the long electric antenna.

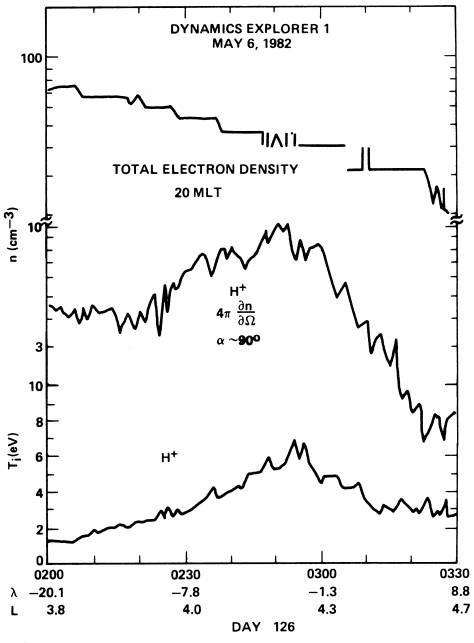

Fig. 16. Summary plot for May 6. 1982.

The electric field spectra at 0242-0245 (prior to the equator crossing), and 0254-0258 (at the equator) are shown in Figure 17. The preequator spectrum (the bottom curve) shows the broad structure normally found at the equator, while the 0251-0258 data (top curve) show a peak which is essentially limited to one channel (185 Hz, while f_{gmg} is 205 Hz). Neither spectra is as intense as the more typical example in Figure 14. The signal at 0254-0258 may be associated with the lower hybrid resonance, rather than the broad spectrum of the equatorial noise, or Bernstein mode. -

ISEE 1 crosses this region at nearly the same time as DE 1. The ISEE 1 data can therefore be used to determine the radial density profile for the DE 1 equator crossing. Figure 18 shows the UHR derived density from the ISEE 1 plasma wave data. The UHR comes on scale at 400 kHz at 2335 UT, drops relatively sharply to 80 kHz from that time until 2400 UT, then changes slope and drops monotonically down to 25 kHz at 0130 UT, as the satellite moves outward. The density profile for this segment is plotted versus "L" in Figure 17. Near L = 4.3, the density profile was fitted with the functional form $n_o(L/4.3)^{-x}$, from L = 3.9 to 5.2. The resulting parameters were n_o = 41 cm^{-3}, x = 4.5. The density value is the same as the equatorial density observed by DE 1 at the equator. For a broader range of L (L = 3.9 to 6) the least square fit (LSF) resulted in x = 4, and a similar density. Using the $L^{-4.5}$ density profile, it is possible to eliminate the "L" dependence of the DE 1 latitude profile. When this is done, it is found that the density is constant from -30° to +10° magnetic latitude, to within the accuracy of the measurements. The result does not change if an L^{-4} profile is used.

This example demonstrates that the density remains constant while the temperature increases by an order of magnitude. The combination of ISEE and DE data also clearly shows that DE is in the region of the plasmapause density gradient while crossing the equator.

STATISTICAL SURVEY

The examples presented above illustrate most of the features found in the plasma data during the equator crossings examined to date. In order to complete the study of the RIMS data, the latitudinal and radial extent of the equatorially trapped plasma were studied for several hundred orbits in 1982, providing a reasonably complete coverage in local time, at varying radial distance. The local dawn sector (0400-0900) is the one region not highly sampled at reasonable (greater than L = 2.5) altitudes. There were approximately 300 orbits where equatorially trapped plasma was found. Overall, the survey resulted in 10,000 one-minute samples. Figure 19a shows the projection in the meridian plane of observations of trapped plasma, for all local times sampled. Figure 19b shows the L-LT segments within 10° of the magnetic equator. The observations basically follow the DE pattern of equator crossings, which fortuitously is similar to the statistical average plasmapause location, with maximum altitude in the dusk region. The occurrence probability is shown in Plate 7a, for a magnetic latitude range of 3. 100. The maximum probability is in the dusk late afternoon region, where there is a nearly unity probability of encountering the trapped plasma. By contrast, in the early morning sector, the probability is closer to 50%.

The distribution of probability with latitude is illustrated for three local time segments: 0000-2400, 1300-1500, and 0100-0300 LT. The latitudinal extent is almost ±30° for the early afternoon region (Plate 7c), narrowing to ± 10° in the early dawn (Plate 7d). On average (Plate 7b), the plasma is trapped within about 10° of the equator. (The red sectors from L = 3.0 to 3.75, 1300-1500 LT in Plate 7c. are an artifact of having only one orbit in those bins, during which there was trapped plasma.)

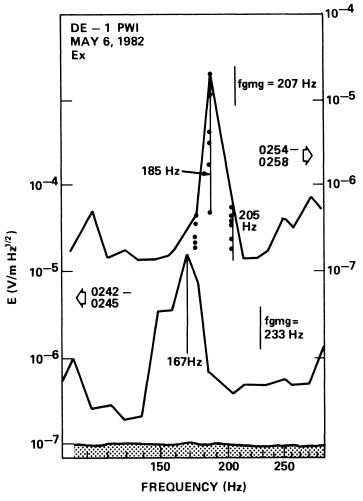

Fig. 17. Electric field frequency spectrum. May 6. 1982.

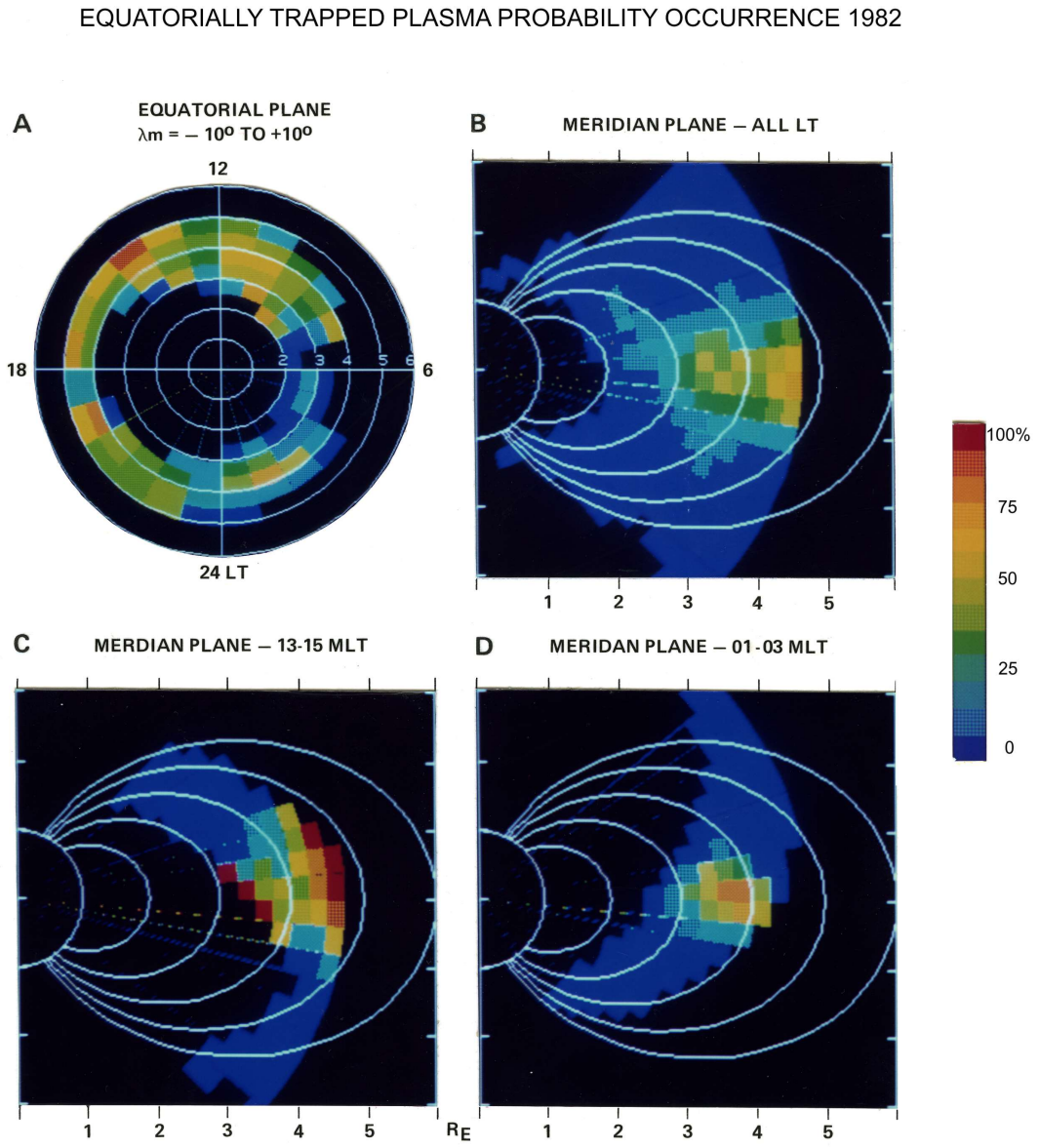

Plate 7. Statistical survey of the occurrence probability of equatorially trapped plasma from the 1982 equator crossings. (a) Probability as a function of local time and L for measurements between ± 10° in magnetic latitude. (b) Probability as a function of magnetic latitude and altitude for all LT. (c) Probability for 1300-1500 LT. (d) Probability for 0100-0300 LT.

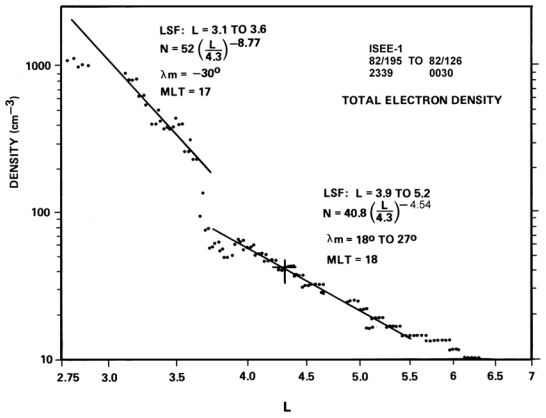

Fig. 18. ISEE-1 density profile, on a log-log scale. Least squares fts (LSF) are done for two segments.

The helium data were included in this study. The trapped H^+ was accompanied by trapped He^+ in the RIMS energy range 41% of the time. There were no cases of trapped He^+ in the absence of trapped H^+.

DISCUSSION

The DE 1 RIMS and PWI observations near the magnetic equator have provided a new perspective on the equatorially trapped plasma and equatorial noise. The polar orbit of DE 1 has allowed us to demonstrate that this region of enhanced temperatures, and 90° pitch angle distributions, is limited to ±5° to ± 10° magnetic latitude in the evening-dawn region, and -1.30° in the afternoon sector. Other examples, not shown here, indicate that within the plasma-sphere, at total plasma densities near 200 cm^{-3}, the latitudinal width can be as small as 2°-3°. The equatorially trapped plasmas occur most commonly in the plasmapause region, where the total densities range from 20 cm^{-3} to 200 cm^{-3}. The opportunity to observe both the core of the ambient ion population, and warm plasma. leads us to infer that we are observing the transverse heating of the core plasma. in order to form the warm. 90° pitch angle distributions. The warm. trapped plasma can comprise 10-90% of the total ion density, so at times the bulk of the ambient plasma is heated. This last characteristic. as found in the second example. is also illustrated by data published by *Olsen et al.* [*1985*]. Plate 1 of that paper illustrates an eclipse passage through the equator, in the plasmapause region. at local midnight. As in the second example from this paper, the satellite eclipse allows improved measurements of the cold, core plasma. Both H^+ and He^+ show a peak in temperature at the equator, though the angular distribution for He^+ remains "rammed." It is not known what happens to the angular distribution of the H^+ due to detector degradation. The observations are consistent with a bulk heating of the core plasma, but with the plasma remaining largely isotropic. Many of the plasmasphere passes have this appearance.

The equatorially trapped plasma is primarily composed of protons. For the five examples shown in this paper, three cases showed He^+/H^+ ratios of 5% to 10%. The example from March 16 (Plate 3) showed no He, while the last example showed that He^+ formed less than 1% of the heated plasma. These examples are representative of the distributions found in all the orbits. When the He^+ ions are heated, the warm He^+ population forms about 10% of the equatorially trapped plasma, the same ratio found in the cold plasma of the outer plasmasphere. About 60% of the time, the He^+ does not participate in the apparent heating process, remaining field-aligned or isotropic. This means that there is no preferential heating of heavy ions associated with the equatorially trapped plasmas, and equatorial noise. This is in contrast to the behavior associated with ion cyclotron waves, as observed on GEOS [*Young et al., 1981*]. In the data analyzed so far, only one case of a heated O^+ component was found, at a relative concentration of 0.1%.

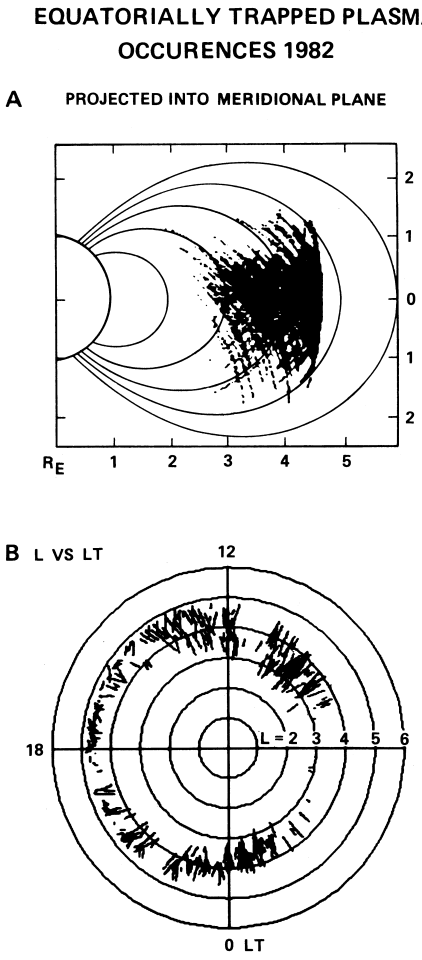

Fig. 19. Statistical summary of equatorially trapped plasma observations, 1982. Each data point is from a 1-min sample, and there is of course substantial overlap in the data points. (a) Meridian plane, all local times. (b) Equatorial plane. L versus LT for 10° magnetic latitude.

The tremendous enhancements in flux encountered at the magnetic equator were initially associated with the idea of density enhancements [*Olsen, 1981*]. The addition of plasma wave data has shown that the equator is not generally a region of enhanced density. The enhancement in ion flux is the result of a temperature increase. There may in fact be a density minimum at the equator. Such examples shown here are associated with sharp spatial boundaries. and the apparent reflection of low-energy field-aligned ions. A further example of such sharp boundaries is given by *Olsen et al.* [*1985*] in Plate 3, where warm plasma is found from the equator up to 10° magnetic latitude, and there is then a sharp boundary leading to a region of colder and denser plasma, even as the satellite rises in altitude. The density minimum may be caused by an increase in the plasma potential, caused by RF heating. Such a potential would explain the apparent reflection of ionospheric flows. An alternate perspective on this process is that the enhanced plasma temperatures at the equator would result in higher plasma pressures, if the ambient plasma density does not decrease. This assumes a requirement for equality in plasma pressure along the field line (in equilibrium).

The statistical survey of the RIMS data provides us with a means of connecting the DE 1 measurements with the previous measurements from ATS 6, ISEE 1, and SCATHA. Before this work, the equatorially trapped plasma was defined by the SCATHA measurements, using an electrostatic analyzer with a low-energy limit of 2 eV. The plasma population was defined to be present when there were highly anisotropic fluxes at energies of tens to hundreds of electron volts, and was nominally found in the outer plasmasphere, or plasmapause region. Typically, the equatorially trapped plasma was found in the dusk bulge in the 5.5- to 7.7-RE range. Such measurements were obtained when the satellite was within a few degrees of the magnetic equator. It appears now that the encounters with warm, dense plasma by ATS 6 in the dusk bulge [*Lennartsson and Reasoner, 1978*] and particularly the "pancake" distributions found in the dayside [*Horwitz and Chappell. 1979; Comfort and Horwitz, 1981*] were measurements of the trapped plasma at 10° magnetic latitude. The higher latitude, altitude. and energy ranges reduced the probability in the late after-noon sector from 90% to less than 25%, but the earlier observations are consistent with the present measurements. Observations with the ISEE 1 mass spectrometer showed that "pancake" H^+ (and He^+) distributions were concentrated near the plasmapause, and close to the equator [*Horwitz et al., 1981*]. These results were limited in latitudinal coverage and did not include the afternoon sector, so direct comparison with our current results is difficult, but it appears that these were also measurements of the high-latitude extension of the equatorially trapped plasma. A substantial effort was made to connect these observations to the plasmasphere filling process, that is, the formation of the plasmasphere after a period of high magnetic activity [*Horwitz et al., 1981a*], and it still seems likely that these observations of trapped plasma are an important clue to the nature of the plasmasphere formation process. Returning to the comparison with the SCATHA data, it now appears that to a certain extent, the extreme localization of the "equatorially trapped" plasma is partly an effect of the energy range studied — i.e., energies of tens to hundreds of electron volts. The peak energies, and most anisotropic distributions, are found within a few degrees of the equator, but the trapped distribution extends substantially along the field line, if it is searched for at sufficiently low energies.

The plasma waves observed at the magnetic equator, and presented in this paper, fall into two categories. The first we term equatorial noise, which has been associated with the broad spectrum of electromagnetic waves which fill much of the frequency range between the proton gyrofrequency and the geometric mean gyro frequency. The high-frequency limit is considered to be the lower hybrid frequency. These characteristics are consistent with the previous identification of these waves as an electromagnetic Bernstein mode, as developed by *Fredericks* [*1968*] and observed by *Russell et al.* [*1970*] and *Gurnett* [*1976*]. A second category is a narrow (1 to 3 channels wide) spectral feature just below the geometric mean gyrofrequency, tentatively identified as a lower hybrid resonance emission.

The nature of the DE 1 plasma wave observations differs significantly from that of the recently reported GEOS observations [*Perraut et al., 1982*]. Their observations were oriented toward the magnetic component in the 0- to 8-Hz frequency range, while the DE 1 observations are primarily of the electric component, with most of the data coming at frequencies above 100 Hz. much like the original Hawkeye and IMP 8 observations [Gurnett, 1976]. The majority of the wave power is apparently in the first few harmonics above the proton gyrofrequency, in the magnetic component, so both sets of observations need to be considered in studies of wave generation, and effects on the plasma.

The generation of the Bernstein mode has been discussed by *Gul'Elmi et al.* [*1975*], *Curtis and Wu* [*1979*], and *Perraut et al.* [*1982*]. The two earlier papers suggest that the energy source is MeV particles, and use relativistic terms in the wave growth calculation. Perraut et al. suggest that the energy source is the 5- to 30-keV ion portion of the plasma sheet, or ring current. They use a spectral feature of the ion distribution function termed the "deep proton minimum" [*DeForest and Mcllwain, 1971*]. This is a minimum in the ion distribution function at all pitch angles resulting from the boundary in energy between eastward and westward convecting ring current ions. A ring current energy source is consistent with IMP 8 observations of a strong $D_{,,}$ correlation for the equatorial noise (T. L. Aggson. private communication. 1983). We hope to investigate the relationship between the 1- to 16-keV measurements from the energetic ion composition experiment (EICS) and the PWI data in the near future.

The possibility that the thermal ions are being heated by the equatorial noise has been discussed by *Curtis* [*1985*]. He invokes stochastic processes to explain the heating, based on the inferences from the original SCATHA electrostatic analyzer observations [*Olsen. 1981*]. The few cases presented here and previously [*Olsen, 1981*] only begin to indicate the likelihood of this interaction, however. An investigation of the statistical relationship between the narrow (LHR) and broad wave features and the RIMS data is under way.

Some perspective on the current observations can be obtained by considering the energy densities in each of the pertinent particle populations, and the observed waves: (1) ring current, 10 keV, 1 cm^{-3}, 10^{-9} J/m^3; (2) thermal plasma, 10 eV, 10 cm^{-3}, 10^{-11} J/m^3; (3) cold plasma, 1 eV, 90 cm^{-3}, 10^{-11} J/m^3; and (4) waves: electric, 10^{-4} V/m, 10^{-17} J/m^3; and magnetic, 10^{-2} γ, 10^{-14} J/m^3. There is substantially more power in the nominal energy source, and in the heated plasma, than in the waves.

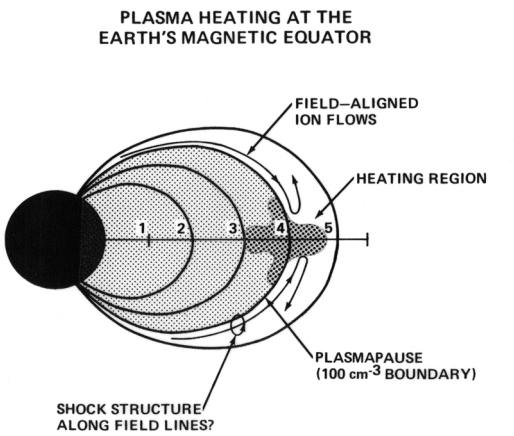

Fig. 20. Summary figure for the equatorial processes inferred from the observations in this paper.

The relatively high energy density in the "heated" plasma does not preclude the observed waves from being the energy source for these ions. It is possible that these waves represent a highly efficient conduit for the transfer of energy from the ring current to the plasmasphere. A wave growth/transport/absorption calculation is substantially beyond the scope of the present work. However, we can use the nature of the Bernstein mode to estimate a heating time. We assume that the waves propagate radially and are limited to ±10° latitude, as indicated by observations and ray tracing calculations (A. Roux, private communication, 1983). Since the Bernstein mode has stop bands at each gyroharmonic, it is limited in the radial distance it can propagate before absorption (or reflection) occurs. If we make the conservative estimate that the frequency at the generation point is at the bottom of the frequency band (large k), and absorption at the top (small k), we then have $f_n(r) = f_{n+1}(r + \Delta r)$ [see *Fredericks, 1968*]. Since $f_n(r) = n \bullet \Omega_n$ and $f_{n+1}(r) = (n+1) \bullet \Omega_n$ we obtain $n \bullet B(r) = (n+1) \bullet B(r + \Delta r)$ or

$$\frac{n+1}{n} = \frac{B(r)}{B(r+\Delta r)} = \left(\frac{r+\Delta r}{r}\right)^3$$

we obtain, for large n, $\Delta r/r = 1/3$ n. For L = 4.5, n = 30, we obtain about 0.05 RE for the propagation distance. For an energy density as noted above, and a power flux of 10^{-9} W/m^2, this results in a heating period of about one hour, which is consistent with the observations.

Our view of these data is summarized in Figure 20. Field-aligned flows from the ionosphere fill the outer plasmasphere, and are thermalized by "shock" processes both along the field line, and at the equator, as suggested by the original polar wind theory of Banks and Holzer [1968]. In this context, the creation of the equatorially trapped plasma may be an element of the plasmasphere filling process. The two hemispheres are separated by the plasmas and potential structure at the equator. It is possible that the filling process begins off the equator, resulting in a region of relative minimum density at the equator which persists through the filling process. The greater latitudinal range of the heated plasma region at the plasmapause is inferred from observations on DE 1, but was initially suggested by T. L. Aggson (private communication, 1983).

In retrospect, we have been fortunate that the plasmapause was found so regularly at L 4.5. A different apogee could have resulted in a much more limited data set. The combination of ISEE and DE data helped substantially in resolving the "L" versus "λ_m" parameters. The next major improvement in our understanding probably depends on the information obtainable from an equatorial ($\lambda_m \leq 3°$) satellite which produces radial profiles, such as the AMPTE/CCE satellite, or the proposed ISTP Equator satellite.

Acknowledgments. We would like to thank the programming staffs of Boeing Corp. and Intergraph Corp., particularly Dick West. Our thanks to the Data Systems Technology Program and the SPAN network for providing the computer resources to analyze the data. This work was supported by NAS8-33982 and NSF ATM8-300426 at UAH, and NAS5-28701 at the University of Iowa.

The Editor thanks two referees for their assistance in evaluating this paper.

REFERENCES

Banks, P. M., and T. E. Holzer, The polar wind. *J. Geophys. Res, 73*. 6846-6854, 1968.

Biddle, A. P., T. E. Moore. and C. R. Chappell. Evidence for ion heat flux in the light ion polar wind. *J. Geophys. Res., 90*, 8552-8558. 1985.

Chappell, C. R., S. A. Fields. C. R. Baugher. J. H. Hoffman. W. B. Hanson. W. W. Wright. H. D. Hammack, G. R. Carignan. and A. F. Nagy, The retarding ion mass spectrometer on Dynamics Explorer-*A, Space Sci. Instrum., 5*, 477–391, 1981.

Comfort, R. H., and J. L. Horwitz, Low energy ion pitch angle distributions observed in the dayside at geosynchronous orbit, *J. Geophys. Res.*, *86*, 1621–1627, 1981.

Comfort, R. H., J. H. Waite. Jr., and C. R. Chappell. Thermal ion temperatures from the retarding ion mass spectrometer on DE 1, *J. Geophys. Res., 90*, 3475–3486, 1985.

Curtis, S. A., Equatorial trapped plasmasphere ion distributions and transverse stochastic acceleration. *J. Geophys. Res., 90*, 1765–1770, 1985.

Curtis, S. A., and C. S. Wu. Gyroharmonic emissions induced by energetic ions in the equatorial plasmasphere, *J. Geophys. Res*., *84*, 2597–2607, 1979.

Decreau, P. M. E., D. Carpenter. C. R. Chappell. R. H. Comfort. J. Green, R. C. Olsen. and J. H. Waite. Latitudinal plasma distribution in the dusk plasmaspheric bulge: Refilling phase and quasi-equilibrium state, *J. Geophys. Res.*, *91*, 6929-6943, 1986.

DeForest, S. E., and C. E. Mcllwain. Plasma clouds in the magnetosphere. *J. Geophys. Res., 76*, 3587–3611, 1971.

Engebretson, M. J., L. J. Cahill. J. H. Waite. D. L. Gallagher. M. O. Chandler. M. Sugiura. and D. R. Weimer, Wave and plasma observations during a compressional Pc 5 wave event August 10. 1982. *J. Geophys. Res., 91*, 6884-6898, 1986.

Fredericks, R. W., Structure of generalized ion Bernstein modes from the full electromagnetic dispersion relation. *J. Plasma Phys.*, *2*, 365-380, 1968.

Gough, M. P., P. J. Christiansen. G. Martelli, and E. J. Gershuny, interaction of electrostatic waves with warm electrons at the geomagnetic equator, *Nature, 279*, 515–517, 1979.

Gul'Elmi, A. V., B. 1. Klaine. and A. S. Potapov. Excitation of magnetosonic waves with discrete spectrum in the equatorial vicinity of the plasmapause. *Planet. Space Sci., 23*, 279-286. 1975.

Gurnett, D. A., Plasma wave interactions with energetic ions near the magnetic equator. *J. Geophys. Res., 81*, 2765–2770, 1976.

Horwitz, J. L., and C. R. Chappell. Observations of warm plasma in the dayside plasma trough at geosynchronous orbit. *J. Geophys. Res*., *84*, 7075–7090. 1979.

Horwitz, J. L., C. R. Baugher. C. R. Chappell, E. G. Shelley, and D. T. Young. Pancake pitch angle distributions in warm ions observed with ISEE 1. *J. Geophys. Res., 86*, 3311–3320, 1981a.

Horwitz, J. L., C. R. Baugher. C. R. Chappell. E. G. Shelley. D. T. Young, and R. R. Anderson, ISEE 1 observations of thermal plasma in the vicinity of the plasmasphere during periods of quieting magnetic activity, *J. Geophys. Res., 86*, 9989–10.001, 1981b.

Kurth, W. S., J. D. Craven, L. A. Frank, and D. A. Gurnett. intense electrostatic waves near the upper hybrid resonance frequency. *J. Geophys. Res., 84*, 4145–4164. 1979.

Lennartsson, W., and D. L. Reasoner. Low energy plasma observations at synchronous orbit. *J. Geophys. Res., 83*, 2145–2156. 1978.

Mauk, B., Electromagnetic wave energization of heavy ions by the electric "phase bunching" process. *Geophys. Res. Lett., 9,* 1163-1166. 1982. Olsen. R. C., Equatorially trapped plasma populations. *J. Geophys. Res., 86*, 11,235–11,245, 1981.

Olsen, R. C., Field-aligned ion streams in the earth's midnight region. *J. Geophys. Res., 87*. 2301-2310, 1982.

Olsen, R. C., C. R. Chappell. D. L. Gallagher. J. L. Green. and D. A. Gurnett. The hidden ion population: Revisited. *J. Geophys. Res.,* 90. 12_,12_1–12.132. 1985.

Perraut, S., A. Roux. P. Robert. R. Gendrin. J.-A. Sauvaud. J.-M. Bosqued. G. Kremser, and A. Korth. A systematic study of ULF waves above f_{H+} from GEOS I and 2 measurements and their relationships with proton ring distributions, *J. Geophys. Res., 87,* 6219-6236. 1982.

Quinn, J. M., and R. G. Johnson. Composition measurements of warm equatorially trapped ions near geosynchronous orbit. *Geophys. Res. Lett., 9*, 777–780, 1982.

Rauch, J. L., and A. Roux. Ray tracing of ULF waves in a multicomponent magnetospheric plasma: Consequences for the generation mechanism of ion cyclotron waves. *J. Geophys. Res.,* 87, 8191-8198, 1982.

Roux, A., S. Perraut. J. L. Rauch. C. de Villedary. G. Kremser. A. Korth. and D. T. Young. Wave particle interactions near Ω_{He}. onboard GEOS 1 and 2. 2. Generation of ion cyclotron waves and heating of He^+ ions. *J. Geophys. Res., 87*, 8174-8190. 1982.

Russell, C. T., R. E. Holzer, and E. J. Smith. OGO 3 observations of ELF noise in the magnetosphere, 2. The nature of the equatorial noise, J. Geophys. Res., *75*, 755-768, 1970.

Shawhan, S. D., D. A. Gurnett. D. L. Odem. R. A. Helliwell. and C. G. Park. The plasma wave and quasi-static electric field experiment (PWI) for Dynamics Explorer A, *Space Sci. Instrum., 5*, 535-550. 1981.

Stix, T. H., The Theory of Plasma Waves. McGraw-Hill. New York. 1962.

Wrenn, G. L., J. F. E. Johnson. and J. J. Sojka, Stable "pancake" distributions of low energy electrons in the plasma trough, *Nature. 279*, 512-514, 1979.

Young, D. T., S. Perraut, A. Roux, C. de Villedary, R. Gendrin, A. Korth, G. Kremser, and D. Jones. Wave-particle interactions near Ω_{He}. observed on GEOS 1 and 2. 1. Propagation of ion cyclotron waves in He^+-rich plasma, *J. Geophys. Res., 86,* 6755-6772. 1981.

R. R. Anderson. Department of Physics and Astronomy, University of Iowa. Iowa City, IA 52242.

C. R. Chappell and D. L. Gallagher. Space Science Laboratory, NASA Marshall Space Flight Center, Huntsville, AL 35812.

J. L. Green. National Space Science Data Center, Greenbelt, MD 20771.

R. C. Olsen. Department of Physics, University of Alabama in Huntsville. Huntsville. AL 35899.

S. D. Shawhan, NASA/HQ/EES, 600 Independence Avenue, S.W., Washington, D.C. 20546.

(Received October 17, 1985;
revised August 19, 1986:
accepted September 18, 1986.)